Reactivity of Supplementary Cementitious Materials (SCMs) in Cement Blends

Jørgen Skibsted[1,*] and Ruben Snellings[2]

[1] Department of Chemistry and Interdisciplinary Nanoscience Center, Aarhus University, Langelandsgade 140, DK-8000 Aarhus C, Denmark

[2] Sustainable Materials Management, Flemish Institute of Technological Research (VITO), Boeretang 200, 2400 Mol, Belgium

* Corresponding author.

Phone: (+45) 2899 2029, E-mail: jskib@chem.au.dk

Abstract

Supplementary cementitious materials (SCMs) are key components of sustainable, low carbon cements. To maximize their use in blended cements, the impact of SCMs on cement hydration needs to be understood and accurately captured by models. A central element in such models is the reactivity of the SCM, which is tedious to measure. Establishing relationships between SCM properties and their intrinsic reactivity is therefore highly important. Moreover, mechanisms enhancing or limiting SCM reactivity in blended cements need to be well-understood. This work reviews recent progress in the description and understanding of the reactivity of SCMs and their impact on Portland clinker hydration. Insights derived from fundamental work using synthetic SCMs, dissolution experiments and model systems are discussed as well as recent work studying the impact of common SCMs on hydration and microstructure of blended cements. Particular attention is paid to recent work on calcined clays, which are currently receiving substantial attention.

Keywords:

Pozzolan (D); filler (D); Granulated blast-furnace slag (D); Blended cement (D); Hydration (A); Dissolution.

1. Introduction

Supplementary cementitious materials (SCMs), used in the cement industry, comprise generally industrial waste products, natural pozzolans and activated minerals that exhibit either hydraulic or pozzolanic properties. As separate materials and in contact with water, most SCMs will not show any significant hydraulic reactions of cementitious value. However, as fine powders and under alkaline aqueous conditions or in contact with calcium hydroxide they will react chemically, *i.e.* 'the pozzolanic reaction', and form hydration products similar to those of cementitious systems. Typical SCMs used by the cement industry are limestone and industrial by-products such as fly ashes from coal-fired power plants, blast furnace slags from pig iron production, silica fume from the ferrosilicon industry, rice husk ashes from production of rice. Moreover, natural pozzolans and thermally activated clay minerals (e.g. metakaolin) can also be used, which along with the industrial by-products are characterized by high contents of silica or silica and alumina. Blast-furnace slags may additionally have high calcium contents, allowing semi-hydraulic reactions to take place in the absence of Portland cement.

Although cement is a low-cost and low-energy product compared to other construction materials, it's extremely large-scale production implies that it is responsible for 6 – 8 % of the anthropogenic CO_2 emissions [1]. Portland cement is by far the most dominant type of cement binder and about 60% of the CO_2 from Portland cement production comes from decarbonation of limestone in the clinkering process. The remaining 40% stems from fuels and electricity used for heating and milling. Thus, reduction of CO_2 emissions associated with cement production represents the most important and urgent challenge for the cement industry. As stated in United Nations recent report on 'eco-efficient cements' [2], there exists no single solution to a sustainable cement production. However, the partial replacement of the CO_2 intensive Portland clinkers by SCMs represents a very attractive approach, as it can reduce CO_2 emissions by up to 30 – 40% without suffering significant changes in strength performance, durability and costs of the material.

The replacement of Portland cement by SCMs is already a widely adopted industrial practice, particularly for limestone, coal combustion fly ashes and granulated blast furnace slags, representing the most commonly used SCMs. Furthermore, the development and characterization of SCMs has been an active research area for at least the past two decades [3-8]. However, the availability of the conventional by-product SCMs varies regionally and they will not be able to cover the global needs for SCMs in the future. In particular, the amounts of fly ashes are decreasing since coal-fired power plants are being phased out for environmental protection purposes in several countries. Thus, there is an urgent need for developments of new SCMs that are comparable or superior to fly ashes and slags. In this context, limestone and clays represent important types of material available in large deposits

all over the world. For this reason, the development of ternary cement blends using a combination of limestone and an aluminosilicate-rich SCM such as calcined clay materials has received significant research interest, for example, as witnessed by three international conferences on `calcined clays for sustainable concrete´ from 2015 – 2019 [9].

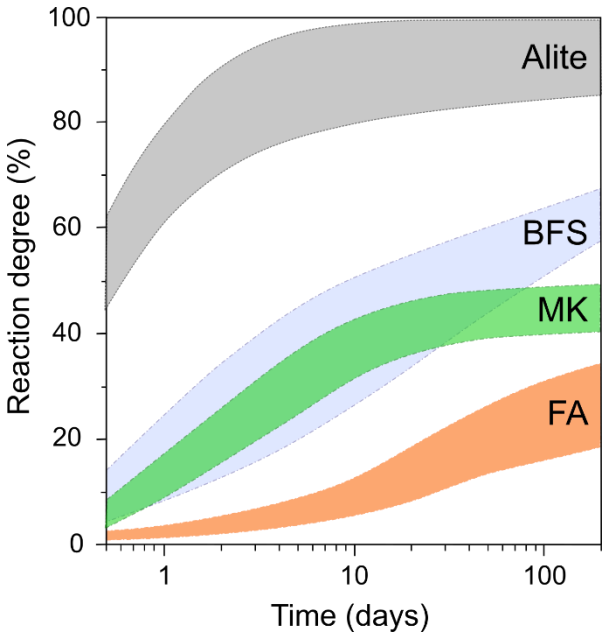

Fig. 1. Degree of reaction envelopes for alite and common SCMs in blended cements, *i.e.*, BFS: blastfurnace slag, MK: metakaolin, FA: siliceous fly ash. The degree of reaction envelopes represent typically reported range of values from a (non-exhaustive) compilation of hydration studies, *i.e.*, for alite [3,10,11], slag [10,12,13], metakaolin [14,15], and fly ash [13,16-18]. Individual data points are omitted for clarity. Clinker substitution levels in the included studies ranged from 30 to 50 wt.%.

The drive towards low-clinker cements with increasing proportion and number of SCMs will lead to the development of more complex, balanced hydrating systems since the presence and reactions of the SCMs influence the hydration kinetics of the clinker phases and the products formed. Generally, the reaction of SCMs is slower than that of the main clinker phase, alite Ca_3SiO_5, as shown in a compilation of reported degrees of reaction for alite and common SCMs in Figure 1 for clinker replacement levels between 30 and 50 wt.%. This results in a decrease in early strength development when the SCM replacement level is increased. It is clear that not all SCMs show similar reaction over time. Metakaolin is well-known to be much more reactive than siliceous fly ash, however, its degree of reaction is limited by the availability of $Ca(OH)_2$. At lower clinker replacement levels metakaolin can reach higher degrees of reaction, *e.g.* up to 100% at 20 wt.% clinker replacement after prolonged hydration [19]. Even within one type of SCM, the variation in reactivity can be quite significant. The reaction of the SCM is reflected in the hydrate phase assemblage, the microstructure and eventually

the performance of the cement. As can be seen in Figure 1, most SCMs continue to react on the long term and for this reason their main contribution to strength development occurs during prolonged hydration. Eventually, this may lead to strengths that can reach or exceed neat Portland cement after 28 to 90 days of hydration. The fact that equivalent performance can be reached, combined with a significantly enhanced sustainability and in some cases improved long-term durability, is driving the development of Portland cement – SCM blends towards increasing substitution levels.

This paper attempts to summarize progress over the last 4 – 5 years in our understanding of reactivity of SCMs and the impact of SCMs on Portland clinker hydration in blended systems. We focus on mechanistic descriptions of SCM dissolution and reaction under neutral and alkaline conditions with main emphasis on physical and chemical parameters affecting the reactivity of SCMs. The availability of different types of SCMs, their impact on cement performance, and durability aspects of concrete based on binary and ternary Portland cement blends are described in more detail in a companion review by Juenger *et al*. [20]. Moreover, the most common SCMs used by the cement industry are also employed as principal phases or major constituents in alkali-activated materials, however, highly alkaline conditions (pH > 14) and alkali-activated SCMs are not addressed specifically in this review. A range of relatively new SCMs are currently being developed for applications in cement blended systems, including rice-husk ashes, calcined dredging sediments, steel slags and natural pozzolans such as volcanic tuffs, ashes and zeolites. Generally, these SCMs are rich in silica or aluminosilicates, which are the principal components in conventional SCMs such as fly ashes, slags, silica fume, glasses and calcined clays. The examples in the present review cover mostly these conventional SCMs. The cement industry faces undoubtedly increasing demands for SCM alternatives to slags and fly ashes, and in this context materials global and local availability should also be considered an important parameter.

2. SCM reaction mechanisms in blended cements

2.1. General reaction mechanisms

SCMs impact the hydration of blended or composite cements in two main ways. Firstly by physical effects that also occur for inert fine powders or fillers, hence the collective term ‘filler effect’ [21,22]. Secondly by taking part in chemical reactions to form hydration products [5,6,8]. This chemical reaction follows a dissolution-precipitation mechanism, the three main components being the solid reactants, the solid hydrate reaction products, and the (pore) solution. For the SCM as a solid reactant, two main types of chemical behavior are distinguished. In case $Ca(OH)_2$ is consumed by the reaction of the SCM, then it is designated as a ‘pozzolanic reaction’. In case the reaction does not require

$Ca(OH)_2$, or $Ca(OH)_2$ acts mostly for pH activation, then it is termed as 'hydraulic' or 'latent hydraulic reactions', respectively.

In blended cements, the pozzolanic and hydraulic reactions of SCMs produce a restricted range of (meta)stable hydrates. If the reaction kinetics of the hydration reactions are known, current thermodynamic models [23,24] and databases [25] succeed to fairly accurately predict the types of hydrates, their quantitative proportions and even variations in their composition for an increasingly wide range of blended cement formulations and hydration conditions. The apparent paucity of products is explained either by the predominance of clinker phase hydration or by the underlying dissolution-precipitation mechanism shared by cement hydration reactions [26].

The aqueous solution, often referred to as 'pore solution', plays a pivotal role as both reaction medium and reactant at the same time. This enables the application of solution thermodynamics to predict which phases will form by minimization of Gibbs energy [5,27]. Thus, the pore solution composition reflects the balance between source and sink term, where the source term is supplied by the dissolution of the solid reactants, and the sink term depends on the precipitation and solubility of the hydration products [28]. This means that for a hydration reaction to occur, the aqueous solution needs to be in disequilibrium or undersaturated towards the reactants, and in equilibrium or supersaturated with respect to the hydration products. Thereby, a larger difference between the solubilities of the reactants and the products will result in an increased driving force and potential to overcome kinetic barriers [29].

2.2. Common SCM reaction schemes

Generally, SCMs consist of the same chemical elements as Portland clinker phases, only their proportioning and combination in the constituent solid phases is different. In consequence the reaction of SCMs in blended cements results in similar hydration products as long as $Ca(OH)_2$ is available. Proportions and composition of the hydration products do shift significantly upon progressive reaction of the SCM. Reaction of a mainly siliceous pozzolanic SCM such as silica fume (S) leads to formation of C-S-H[1]:

$$\mathrm{S} + 1.7\ \mathrm{CH} + 2.3\ \mathrm{H} \rightarrow \mathrm{C_{1.7}SH_4} \tag{1}$$

For aluminosilicate SCMs, such as metakaolin (AS_2), also calcium aluminate hydrates appear in the reaction equation, the type depending on the counter-anion, for instance monosulfoaluminate in the case of stoichiometric calcium sulfate ($C\bar{S}$) availability:

[1] Conventional cement nomenclature: C = CaO; S = SiO_2; A = Al_2O_3; F = Fe_2O_3; H = H_2O; $\bar{S}$ = SO_3; $\bar{C}$ = CO_2.

$$\mathrm{AS_2} + 6.4\ \mathrm{CH} + \mathrm{C\bar{S}} + 13.6\ \mathrm{H} \rightarrow 2\ \mathrm{C_{1.7}SH_4} + \mathrm{C_4A\bar{S}H_{12}} \quad (2)$$

For systems where calcium carbonate ($\mathrm{C\bar{C}}$) is present in the blended cement, calcium carbo-aluminate hydrates form instead of monosulfoaluminate and the balance sulfate will precipitate as ettringite:

$$\mathrm{AS_2} + 6.4\ \mathrm{CH} + 0.5\ \mathrm{C\bar{C}} + 1.5\ \mathrm{C\bar{S}} + 23.1\ \mathrm{H} \rightarrow 2\ \mathrm{C_{1.7}SH_4} + 0.5\ \mathrm{C_4A\bar{C}H_{11}} + 0.5\ \mathrm{C_6A\bar{S}_3H_{32}} \quad (3)$$

Comparing Eqs. 2 and 3, it is apparent that the combined use of Al-rich SCMs and limestone enables to bind more water into solids [3,30], a reaction scheme which is exploited in a new generation of ternary blended cements such as limestone – fly ash – cements [31], limestone – slag – cements [10], or limestone – calcined clay – cements [32]. When the SCM contains magnesium and aluminium as in the case of blast furnace slag, hydrotalcite is formed as additional reaction product. As latent hydraulic SCM, blast furnace slag consumes less $Ca(OH)_2$ and can thus reach a higher degree of reaction before $Ca(OH)_2$ is depleted [10,28], *c.f.*, comparison between metakaolin and slag in Figure 1.

An important shift in product assemblage and pore solution composition occurs upon depletion of $Ca(OH)_2$. $Ca(OH)_2$ acts as a buffer for both Ca and pH, and depletion of $Ca(OH)_2$ by the pozzolanic reaction therefore leads to a lowering of pH of the system, falling Ca/Si ratio in C-S-H and formation of strätlingite as hydration product (C_2ASH_8) in cases of Al-rich SCMs [19,33]. It should be noted that only blended cements containing highly reactive SCMs such as metakaolin or silica fume, or very high clinker replacement levels reach the point of $Ca(OH)_2$ depletion [34,35].

2.3 Mechanisms limiting SCM reactions

Most SCMs in blended cements fail to reach full reaction, even over long time periods. The mechanisms that limit the SCM reaction to reach completion are still not entirely resolved and debated, although there is consensus that a combination of thermodynamic and kinetic barriers are laying at the base. One reason is that at high degrees of hydration a reducing availability (activity) of reactants ~~including~~such as $Ca(OH)_2$ or water can no longer drive the reaction.

2.3.1 Water availability

The availability of water is essential to the hydration of SCMs in a Portland cement environment. From a thermodynamic perspective most common blended cement-based products contain sufficient water to achieve full hydration of all reactants, however, this is rarely reached in practice. Achieving full hydration is hindered by a number of kinetic barriers, amongst which are pore structure refinement and space limitations, but obviously also reducing activities of the main

reactants, *i.e.* the portlandite ($Ca(OH)_2$) as mentioned above, the SCM, but also water. In this respect, it is well-known that consumption of water by cement hydration reduces the concrete internal relative humidity leading to generation of capillary pore pressure and shrinkage [36]. A decreasing water activity or relative humidity can effectively reduce or stop hydration of clinker minerals as shown in recent experiments on C_3S hydration in mixed solutions of isopropanol and water [37,38]. The relative humidity at which a hydration reaction can no longer proceed depends on the driving force. In case of C_3S, hydration stalls between 70 to 80% RH [39]. Less vigorous reactions such as hydration of C_2S require a higher relative humidity to proceed and will be phased out once more reactive phases such as C_3S hydration has reduced water to below the threshold relative humidity. Water activity also depends on the ionic strength of the solution, in cement pore solutions dominated by soluble alkalis [28]. At a pH of 14 or lower, water activity in cement pore solutions is very close to unity. However, at very high NaOH concentrations of 2 M and higher, as used in some alkali-activated cements, water activity decreases because of the increased need for solvation of the ionic species leaving fewer water molecules to take part in the dissolution and hydration reactions. Maraghechi *et al*. [40] measured decreasing dissolution rates of soda lime glass above a pH of 14 explaining this by increasing surface charge or decreasing water activity with increasing pH. Overall however, few literature data are available on the dependence of SCM reactivity in blended cements on water activity to complement or confirm the observations made for C_3S and soda lime glass.

2.3.2 Space availability

Another reason stems from the availability of pore space for hydrates to precipitate in. During hydration initial porosity is filled by solid hydration products and the pore size distribution becomes finer. Pore structure refinement is particularly important for blended cements and one of the main reasons behind the enhancement of durability properties. Growth of hydrates inside the increasingly refining pores is restrained as the hydrates cannot grow beyond a certain size or in preferred directions to reduce surface energy. Therefore an increasingly larger driving force is needed to sustain hydration. At constant pressure, the relationship between driving force (ΔG) or supersaturation and crystal size, expressed as the ratio of surface over volume or the surface curvature (dA/dV), is classically expressed by the Ostwald-Freundlich equation [41]:

$$\Delta G = RT \ln\left(\frac{K}{K_{sp}}\right) = \gamma_{cl} v_m \left(\frac{dA}{dV}\right) \tag{4}$$

where R is the universal gas constant, T is the absolute temperature, γ_{cl} is the interfacial energy, v_m is the molar volume of the hydrate, K is the ion activity product and K_{sp} is the equilibrium solubility

product. This relationship is conventionally used to explain coarsening or ripening of crystals or salt crystallization in pores [41], but it can also provide insight in the relationship between confined growth or pore structure refinement and driving force [42]. Following this hypothesis, the cement pore structure refinement should depend on the driving force or the reactivity of the remaining reactant phase assemblage. The higher the reactivity, the larger the reduction of the porosity and the smaller the critical pore radius. Recent work by Scrivener and co-workers showed reachable critical pore radii for slag and fly ash blended cements to be in the range of 6 - 8 nm [18], for calcium sulfoaluminate cement 3 - 4 nm [43] and for ultrahigh performance concrete with remaining C_3S 2 - 3 nm [44]. The differentiation would reflect differences in driving force. Although more research is required to determine both physical properties such as hydrate interfacial energies and the hydrate growth mechanism, Eq. 4 effectively shows that supersaturation needs to increase exponentially to balance the increase in surface free energy for precipitate clusters decreasing in size from 20 nm down to 2 nm diameter, for reasonable interfacial energies of 40 - 120 mJ/m^2 [45].

The effect of SCM reaction in blended cement at later hydration ages has been investigated by Berodier and Scrivener for SCM (slag/fly ash) – quartz – OPC blends, employing a fixed OPC replacement level (40 vol%) and a fixed water/solid volume ratio [18]. Using different SCM:quartz ratios, it was possible to separate effects from cement hydration and SCM reaction. After prolonged hydration (28 - 90 days), the cement hydration was not affected by the SCM content, whereas the degree of SCM reaction decreased with increasing SCM:quartz ratio. From mercury intrusion porosimetry (MIP) and microscopic investigations, it was found that the SCM reaction at later ages was limited by space availability by the absence of water-filled capillary pores [18]. A limiting critical pore entry radius of 6 to 8 nm was associated with this confined growth of hydration products. This effect was further supported by experiments with increased water/solids ratio, resulting in more space available, which postponed the reduction in SCM reaction. The space availability effect was shown to have the highest impact for blended cements with high SCM replacement levels, as also demonstrated in a study of OPC – calcined clay limestone blends with a 50 wt% OPC replacement by Avet and Scrivener [42]. In this system, the formation of carboaluminate hydrates is limited at a certain age by the absence of pores above a critical size. As a consequence, a significant increase in the amount of aluminum incorporated in the C-(A)-S-H phase was observed at this stage, provided by an increase in aluminate concentration in the pore solution from the continuing metakaolin reaction [42].

3. SCM properties affecting reactivity

Continuous progress is being made in better understanding the mechanisms, parameters and properties that control SCM reaction kinetics in blended cements. For SCMs in general, a distinction

can be made between intrinsic SCM properties such as composition and surface area, and extrinsic systems properties such as temperature or solution composition. Changing SCM properties, such as surface area by grinding or thermal history by controlled cooling, are instrumental in increasing SCM intrinsic reactivity. Other common approaches are to activate SCMs by modifying external conditions such as the temperature or the solution composition, e.g. increasing pH by alkali activation in so-called hybrid cements. A more recently proposed approach is activation by counter-anion additions such as carbonates and sulfates to form hydrates of lower solubility with the aim of increasing the driving force and reducing the activity of inhibitors such as aluminate species [10,46]. This section reviews recent progress in our current understanding of how SCM properties affect their reactivity, both in model systems and real blended cements.

3.1 Physical SCM properties influencing reactivity

The fineness of the SCMs has impact on the reaction kinetics of the SCM particles as SCM dissolution increases with increasing surface area. Moreover, the number of nucleation sites for hydrate precipitation and growth increases with a reduction in SCM particle size, which may accelerate the hydration process for both the SCMs and clinker phases at early ages. This has directed research towards the use of nanoparticles in cement blends, in particular nano-silica [47-50] and nano-alumina [51,52]. However, difficulties in dispersion of nano-sized particles in the cement matrices may occur and the water demand will increase with increasing specific surface area for a given SCM [53-55]. For example, the dosage of nanosilica in Portland cement can be optimized to promote early-age strength and this effect can be related to the specific surface area of the nanosilica particles, as accounted for in a quantitative hydration model that considers interparticle interactions [52]. Additionally, the presence of SCMs in blended cements increases the early hydration of the cement phases by the filler effect [21,22], which provides additional space for the formation of hydration products, because of the effectively lower water-to-clinker ratio.

The pore solution (pH) of the cements has an important effect on SCM dissolution kinetics and the extent of the reaction in blended cement matrices. Generally, the alkalinity of the pore solution increases during the early stage and first few days of hydration. Consequently, the reactivity increases with increasing fineness or surface area of the SCM which may reflect a higher propensity of aluminosilicate phases to dissolve in the pore solution of the hydrating cement. This has been shown for a series of green glass cullets (siliceous glass rich in Na and Ca), each with a narrow-range particle size, for which the dissolution of aluminum and silicon increased significantly for the finest fraction (0 – 25 μm) in leaching experiments when pH was 12.5 and above [56]. The Si and Al contents in solution exhibited an approximate linear relationship with the surface area of the glass cullet particles. This could also account for the changes in reaction kinetics and compressive strengths observed for

different cullet glass fractions in blends with Portland cement (25 wt% replacement). An increased reactivity with decreasing particle size has also been observed for samples of the natural pozzolan, pumice, in reactivity tests with calcium hydroxide [57]. In contrast to other SCMs, pumice is an amorphous, porous low-density volcanic rock, rich in silicon and with minor contents of aluminum and alkalis, for which the porous nature may provide additional nucleation and growth sites in the early stages of hydration. For pumice-containing Portland cement mortars (20 wt.% replacement), isothermal calorimetry has shown that finer pumice particles results in enhanced nucleation and growth of hydration products. This results in an increased early-age compressive strength that may compensate for the dilution effect caused by the replacement of the cement with a slower reacting SCM [57]. Moreover, it was found that the beneficial effect of the fine pumice particles on the initial strength development diminishes with time, resulting in materials with similar strengths after prolonged hydration.

The effect of mono-sized SCMs with different particle sizes on the compressive strength of binary Portland cement pastes incorporating fly ash, slag (GBFS) and quartz as SCMs at different replacement levels has been addressed in a recent study [58]. The SCM contributions to the compressive strength were divided into an inherent characteristic effect, a particle-refinement effect, and a hydration effect. The inherent effect depends on surface texture, roughness and the nature of the SCM whereas the hydration effect accounts for the hydraulic/pozzolanic reaction of the SCM in the cement blend. Both the particle-size refinement effect, resulting in a more homogeneous interface between the particles in the blend, and the hydration effect increased with decreasing particle size. An empirical model was proposed for the compressive strength where both contributions exhibit an exponential dependency on the particle size, as expressed by the volume median particle size (D_{50}) and analyzed for pastes with D_{50} = 2 – 90 μm for the SCMs [58]. Obviously, the contribution from the hydraulic reaction is much larger than the particle-size refinement. This effect was more pronounced for the slag with a higher degree of reaction as compared to the FA.

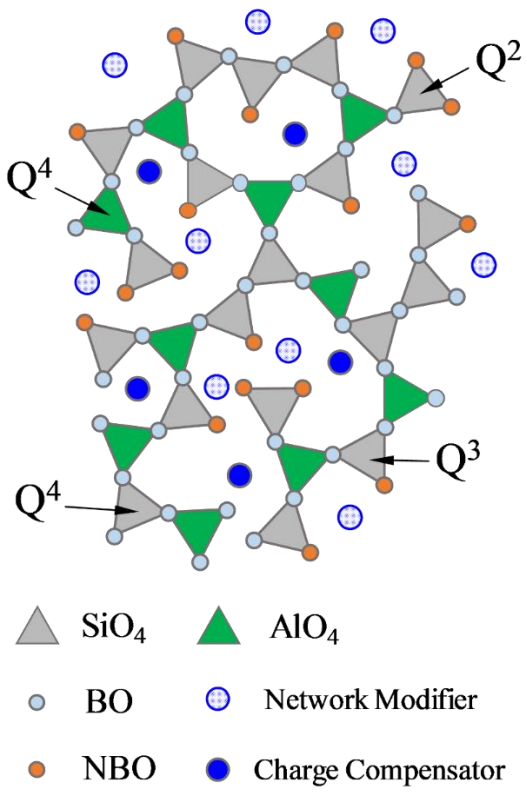

Fig. 2. Schematic two-dimensional illustration of the disordered structure for an aluminosilicate glass composed of network-forming SiO_4 and AlO_4 tetrahedra connected via bonding oxygens (BO). Other cations act as charge-balancing ions or network modifying ions, the latter resulting in non-bonding oxygens (NBO) and thereby a depolymerization of the network. The degree of polymerization (Q^n) is indicated for some of the tetrahedral units.

3.2 Chemical parameters influencing SCM reactivity

The reactive components in SCMs are generally glassy or amorphous phases and their intrinsic reactivity is largely determined by the chemical composition and structure of these components. For fly ashes and slags, the main reactive phases are aluminosilicate or calcium aluminosilicate glasses, respectively, with minor fractions of MgO, Na_2O, K_2O and Fe_2O_3 incorporated. The glass phase is generally composed of acidic silicate (SiO_4) and aluminate (AlO_4) tetrahedra bonded together in a polymerized network by covalently bonded bridging oxygens (Fig. 2). Ca^{2+} and other alkali or earth alkali ions act either as charge-compensating ions or as network-modifying ions. The latter type of ions disrupts the aluminosilicate network, resulting in non-bridging oxygens (NBO) that form ionic bonds with the modifier cations. The glass polymerization degree is often expressed as the fraction of network modifying ions relative to the network forming providing measures for the hydraulic and basicity properties of the glasses. For example, that is the (CaO + MgO)/SiO_2 ratio or NBO/T, the number of non-bridging oxygen atoms relative to oxygens in tetrahedral coordination. These indices

can be linked to the reactivity of the glasses, where lower degrees of polymerization generally result in higher reactivity [59-62].

Calcium aluminosilicate (CAS) glasses, synthesized from pure reagents, are widely used as model compounds for the reactive phases in slags and fly ashes and used to explore their reactivity in terms of composition, structure, dissolution rate and characteristics, alkalinity, temperature and water availability. For example, Durdzinski *et al*. have examined two calcareous fly ashes by SEM-EDS analysis and identified four distinct glass phases with characteristic compositions of a silicate-rich glass, a calcium silicate phase, an aluminosilicate and Ca-rich aluminosilicate glass, respectively [63]. In a subsequent study, they synthesized model Ca-Mg-Na-Al-Mg glasses, targeting these compositions, and analyzed their pozzolanic reactivity in NaOH solution (pH = 13.2) and in Portland cement paste (55 wt% PC – 45 wt% glass blends) [64]. From the batch dissolution experiments at alkaline conditions, they found that the dissolution rate is related to the chemical composition of the glasses. The consumption of the model glasses in the blended cements, as determined by SEM-EDS image analysis, followed the same trends as the rates from the dissolution experiments. A clear and nearly linear increase in intrinsic glass reactivity with the depolymerization of the glasses (NBO/T) was observed, suggesting that the reactivity of fly ashes can be related to the chemical compositions of the constituent glass phases [64]. Using a similar SEM-based quantitative approach, Aughenbaugh *et al.* have investigated four commercial fly ashes (class F) [65]. They found that despite differences in bulk oxide contents, the fly ashes consist of glass phases with similar compositions, *i.e.*, aluminosilicate and calcium aluminosilicate glasses, a mixed-phase glass and an iron-rich glass. The fly ashes contained also minor quantities of quartz, lime and iron oxides, as revealed by X-ray diffraction. These phases were also included in the SEM mapping analysis, which do not distinguish between glassy and amorphous phases. Thus, care should be exercised to exclude inert phases when hydraulic or basicity indices (as mentioned above), calculated based on bulk oxide compositions, are used to predict SCM reactivities of multiphase systems such as slags and fly ashes.

The roles of Ca and Al on the reactivity of CAS glasses mimicking the composition of industrial fly ashes and slags have been addressed in a recent study by Kucharczyk *et al*. [66] where ^{27}Al and ^{29}Si MAS NMR was used to model the structural fragments and bondings in the studied glasses. In this model, aluminum in tetrahedral coordination is considered as a network-forming component whereas five- and six-fold coordinated Al may act as network modifying units. For the CAS glasses with slag or Ca-rich fly ash compositions, more than 90% of Al was present at tetrahedrally coordinated Al sites, implying that most of the aluminum atoms are network formers. The glass reaction was investigated for glass paste samples including limestone and calcite at high pH, which were analyzed by calorimetry, TGA, XRD with PONKCS calculation as well as ^{27}Al and ^{29}Si MAS NMR. The degrees of glass reaction from the XRD and NMR analyses were consistent with

thermodynamic modelling and showed an increased rate of reaction with increasing calcium content whereas the aluminum content has a less pronounced impact [66]. The latter observation may reflect that only a minor part of the aluminum (*i.e.*, five- and six-fold Al) contributes to the depolymerization of the network, although a weakening of the glass structure occurs with an increasing Al network forming content. Enhancement of slag reactivity by modifications in slag composition or cooling rates has been actively investigated over recent years, in particular for slags other than typical ground granulated blast-furnace slags (GGBFS) used as SCM in cement. Increasing the CaO content of iron-silicate slag residues (CaO_x–FeO_y–SiO_2) from non-ferrous metallurgy was shown to result in higher slag reactivity, both as SCM and as precursor for alkali activated materials [67]. Similarly, increasing the CaO content for stainless steel slags resulted in formation of more reactive high temperature phases such as C_3S instead of γ-C_2S [68]. High cooling rates have a generally positive effect on slag reactivity, as it can be linked to either a high glassy phase content or to preservation of more reactive high-temperature crystalline phases such as β-C_2S instead of γ-C_2S. This was demonstrated for different types of steel slags and non-ferrous slags by Pontikes and co-workers [69,70]. Partial crystallization or unmixing of two compositionally different glasses may occur when cooling rates close to the critical cooling rate are used (*i.e.*, the minimum cooling rate to obtain an entirely vitrified solid). Interestingly this may lead to increased reactivity of the glass by concentration of constituents that render the glass less soluble such as Fe_2O_3, MgO or TiO_2 by selective crystallization or separation. This was postulated recently by Kinnunen *et al*. for alumina-rich glasses, simulating re-melting of basaltic stone wool [71].

3.2.1 Introduction to mineral and glass dissolution kinetics

The kinetics of mineral and glass dissolution has been studied intensely in the fields of geochemistry and nuclear waste storage to enable modelling and prediction of mineral reactions such as atmospheric or soil weathering or contaminant release rates from vitrified nuclear waste over geologic timescales [72-74]. This work delivered insightful concepts and models that can be very instrumental in better understanding and eventually modelling what mechanisms and parameters drive and control dissolution of SCMs in cement. As an introduction to a review of recent work on the topic in the cement science community, a brief overview of the main concepts in silicate dissolution developed in geochemistry is given first.

The driving force ΔG behind a dissolution reaction is the disequilibrium between solution concentrations and the solubility product of the solid phase, expressed as the ratio of the ionic activity product (K) to the solubility product, K_{sp} (eq. 4), or solution saturation. Following transition-state theory (TST), the relationship between ΔG and the dissolution rate r is expressed as [75,76]:

$$r = k_{+}\ \Pi(a_j)^{mj}\ (1\text{-}\exp(\text{-}\Delta G/RT)) \quad (5)$$

where k_+ is the forward rate constant, and a_j is the activity of species *j* in the rate-determining reaction. This so-called linear rate equation was used to accurately describe the kinetics of dissolution of quartz and other silica phases over a wide range of temperatures and pressures [77,78]. However, many minerals have a dissolution behavior which cannot be fitted by the TST model, showing strongly sigmoidal dependencies with very low dissolution rates close to equilibrium (saturation) [79,80] (Fig. 3). Modifications to the TST law were made to reflect different rate dependencies for different dissolution regimes, *i.e.*, rapid dissolution by etch-pit nucleation at dislocations under far from equilibrium conditions and slow dissolution by step restart at pre-existing surface topographies [81, 82].

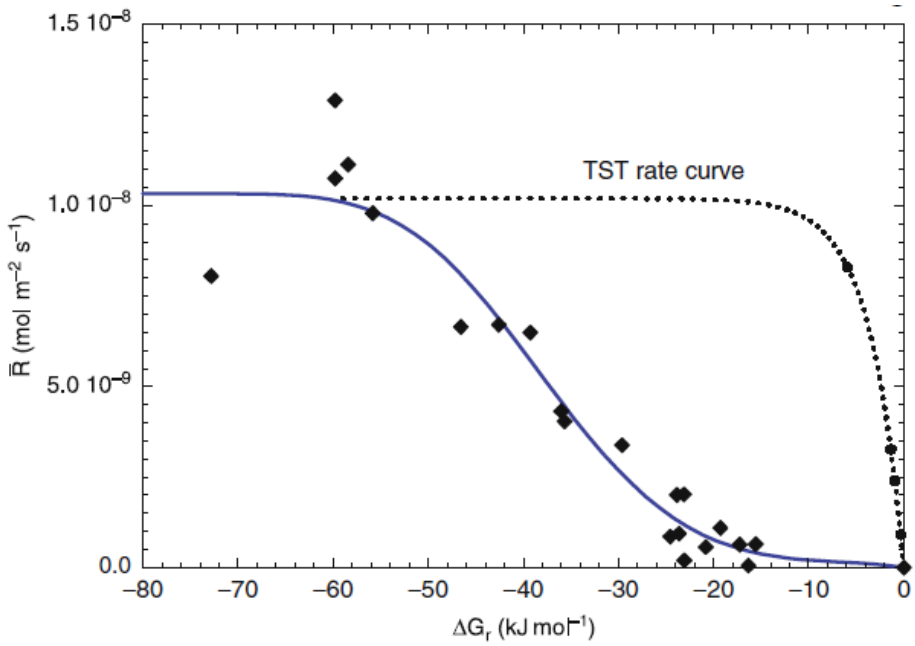

Fig. 3. Measured rates of albite dissolution (diamonds), as a function of driving force (ΔG), shows sigmoidal behavior (fitted line), strongly deviating from the TST rate curve, plotted as dotted curve. Reproduced with permission from ref. 80.

At constant undersaturation, dissolution rates were observed to depend strongly on solution composition, in particular solution pH [83,84]. The pH effect was explained early on by surface (de)protonation that polarizes metal-oxygen bonds and weaken the bonding with the underlying lattice. The concentration of such (de)protonated surface species is a function of pH and directly related to the dissolution rate. In this case the dissolution rate equation in alkaline conditions becomes [73]:

$$r = k_{OH}\, a_{OH}^{m}\ (1\text{-}\exp(\text{-}\Delta G/RT)) \quad (6)$$

where m is referred to as the partial order of reaction that varies as a function of phase composition. This model enables to describe the pH dependency of simple (hydr)oxides such as quartz or gibbsite rather well [74]. However, it cannot explain the dissolution of more complex multioxide materials such as feldspars. In subsequent work, it was found that for many multioxide materials also the effect of ions other than protons or hydroxides needed to be accounted for [85]. For minerals and conditions in which dissolution leads to preferential release or leaching of alkali, alkaline earth or other cations leaving behind a protonated, yet by bridging oxygens interconnected silica surface layer, the model proposed by Oelkers and Schott [74,86] predicts that the dissolution rate depends on the activity of the leached cation in solution. For phases where the residual silica in the leached layer is not interconnected, there is no dependency of the dissolution rate on leached cation concentration in solution. For far from equilibrium dissolution of silicates containing cation M_i, the following general rate equation is proposed [86]:

$$r = k \prod_{i=1, i \neq k}^{i} \left[\frac{K_i \left(\frac{a_{H^+}^{v_i}}{a_{M_i}^{v_i}} \right)^s}{\left(1 + K_i \left(\frac{a_{H^+}^{v_i}}{a_{M_i}^{v_i}} \right)^s \right)} \right] \tag{7}$$

where k is the rate constant and K_i is the equilibrium constant for the exchange reaction between protons and the metal cation M_i. The parameters v_i and s are stoichiometric coefficients for the exchange reaction. To date this model explains dissolution of the widest range of phases and minerals, ranging from basaltic glass [87] over kaolinite ($Al_2Si_2O_5(OH)_4$) to anorthite ($CaAl_2Si_2O_8$) or Mg-olivine (Mg_2SiO_4) [86], all of which are major rock-forming minerals that bear chemical and structural resemblance to common SCM constituents such as vitrified slags, metakaolin, gehlenite or γ-Ca_2SiO_4 (Ca-olivine).

Next to constituent cations, also cations and (organic) anions that are not part of the dissolving phase can affect dissolution kinetics. This effect can be indirect, for instance by decreasing the activity in solution of a constituent cation by complexation, or by changing the pH [88,89]. However, also direct interaction of ionic solutes with the mineral-water surface can strongly affect dissolution rates. For instance, quartz and amorphous silica dissolution rates increase by two orders or magnitude in the presence of low solution concentrations of alkali or alkaline earth cations [90]. In contrast, dissolved aluminium is well-known to inhibit silicate dissolution [91,92]. Aluminate anions, like other bi- or tridentate anions such as phosphate or borate, are thought to slow dissolution by strongly bonding to reactive surface sites through formation of multi-nuclear inner sphere surface complexes, *i.e.* formation of multiple chemical bonds [93]. These strongly attached surface complexes shield off

the surface from further dissolution. As both surface charge and solution speciation are strongly dependent on pH, also formation of surface complexes and the resulting inhibitory or acceleratory effects change with pH. For example, inhibition of quartz dissolution by dissolved aluminate was observed to decrease at pH above 13, related to increased competition in surface adsorption between aluminate and hydroxyl anions [92].

The temperature dependence of dissolution rate constants is mostly described by the apparent activation energy, E_a, as derived from the Arrhenius equation:

$$k(T) = k(T_0)e^{-(E_a/RT)} \tag{8}$$

While ab initio calculations clearly predict an increase in E_a with silicate framework connectedness (number of bridging oxygens per silicate tetrahedron) [94,95], this trend is not clearly followed by experimental observations that show a levelling off for E_a beyond a connectedness of 2 [73]. This is interpreted as rate-control by dissolution of Q^2 or less connected sites at edges, rather than direct dissolution from a perfect surface (Q^3). Activation energies for silicate phase interfacial dissolution were measured to be between 50 to 100 kJ/mol [96].

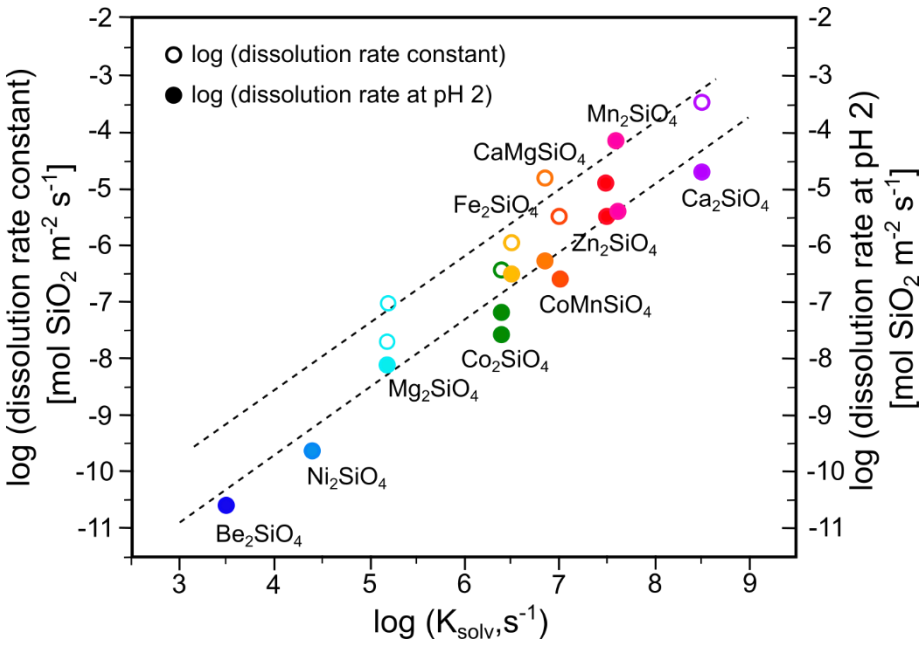

Fig. 4. Correlation between dissolution rates of Q^0 silicates of different composition measured at pH 2 (filled circles), dissolution rate constant (open circles) and the logarithm of the rate constants for water exchange around the cation in solution. Modified after [73].

logarithm of the rate constants for water exchange around the cation in solution. From ref. [73].

In terms of dependency of silicate dissolution rates on phase structure and composition, a compiled database [96] shows the following: (*i*) the dissolution rates strongly increase with decreasing number of bridging oxygens per silicate tetrahedron (connectedness), and (*ii*) for the same connectedness the dissolution rate varies in line with the rate of water exchange of the charge balancing cation in solution. For example, for Q^0 silicates the dissolution rates increase from Mg-olivine (forsterite), over Fe-olivine (fayalite) to Ca-olivine (γ-Ca_2SiO_4), reflecting the strong coordination of hydration shell water by Mg^{2+}, as compared to Fe^{2+} and Ca^{2+} [97] (*c.f.* compiled data in Fig. 4).

3.2.2 Mineral and glass dissolution studies of SCM constituents

Glass dissolution rates, in far from equilibrium conditions and in the absence of hydration products, have been determined by measuring the dissolved concentrations of Ca, Si and Al as function of time for glass powders with a well-defined particle size embedded in alkaline solutions, using liquid-to solid ratio at 1000 or above in batch or flow through reactors [98-100]. By this approach and for calcium aluminosilicate (CAS) glasses covering the compositional range for blast furnace slags over fly ashes to silica fume, Snellings has investigated the initial glass dissolution rates as a function of the initial solution composition of Al, Ca, and Si at pH = 13 [98]. For all glasses in pure 0.1 M NaOH, a congruent dissolution of Al and Si was found whereas Ca was preferentially released for glasses with a CaO/Al_2O_3 molar ratio of 1.0 while Ca was released congruently for the BFS-type glasses. Moreover, the highest glass dissolution rates were observed for the BFS glasses and the rates decreased with decreasing Ca content, corresponding to a linear increase in the logarithm of the dissolution rates and the molar Ca/(Al + Si) ratio for the glasses [98]. Increasing solution concentrations of either Al or Ca resulted in a decrease in glass dissolution rate whereas no effects of increasing Si concentration were observed. The highest dissolution rates for the percalcic (CaO/Al_2O_3 > 1) BFS glasses reflect the surplus of Ca^{2+} ions for charge-balancing the replacement of Si^{4+} by Al^{3+} ions, resulting in a depolymerized network structure composed mainly of Q^2 and Q^3 tetrahedral units. The surplus of Ca^{2+} ions levels off when the CaO/Al_2O_3 = 1.0 line in the CAS phase diagram is approached, corresponding to the presence of nearly fully condensed network structures (Q^4 units) and lower dissolution rates. Similar dissolution experiments at pH = 13 (0.1 M KOH solution) have been reported by Schöler *et al*. for eight glasses with compositions of type F (Si-rich) and C (Ca rich) fly ashes as well as blast furnace slags, where all syntheses incorporated minor constituents of Fe_2O_3, MgO, Na_2O, K_2O and TiO_2 [101]. Overall, the highest dissolution rates were observed for the Ca-rich slags and the lowest rates for the siliceous fly ashes, in agreement with the relation between CaO

content and dissolution found by Snellings [98]. However, Schöler *et al*. observed also that an increasing Al_2O_3 content also results in faster dissolution, reflecting that a fraction of Al_2O_3 acts as network modifier and not only a network-forming oxide. A linear relationship between the initial dissolution rate and the NBO/T ratio for the studied glasses was observed, assuming that an equal fraction of Al_2O_3 and Fe_2O_3 acts as network modifiers in the Ca-rich fly ashes and slags in the calculation of the NBO/T ratios [101]. The pozzolanic activities of the glasses were further studied in model systems of glass powder, portlandite and calcite with a water/solid ratio of 1000 and in blended cements of OPC and glass powder (50:50) with a water/solid ratio of 0.5. The glass reactions in both series of experiments were followed with time by calorimetry and differential thermogravimetry, the latter providing information about bound water and portlandite consumption. The results showed an increasing degree of glass reaction for the Si-rich fly ashes, the Ca-rich fly ashes and the slags, respectively, and also higher reaction for the slags and Si-rich fly ashes with a high Al_2O_3 content. Thus, these data support the dissolution results and thereby that the degree of glass network polymerization, as estimated from the chemical composition, is a main factor affecting glass reactivity under highly alkaline conditions [101].

The temperature dependence of the dissolution in dilute solutions at high pH was investigated by Maraghechi *et al*. [40] for soda-lime glass at 1 M NaOH and 20, 40, 60 and 80 °C. Similarly, Snellings *et al*. [102] have studied GGBFS, fly ash and a silica-rich natural pozzolan at 0.1 M NaOH for 20, 30 and 40 °C. The calculated apparent activation energies range from 55 kJ/mol for GGBFS, to 86, 88 and 95 kJ/mol for fly ash, soda lime glass and natural pozzolan, respectively. Given the significant differences in experimental procedures, the results are quite close and in line with the literature data on dissolution experiments. Moreover, the activation energy values generally increase with silica content or connectedness, as expected from ab initio calculations on silicate dissolution [94,95]. The activation energies from dissolution experiments are higher than typically reported for blended cements [103]. This could be related to the weight accorded to the early hydration period for most calculation methods for blended cements, when the hydration is dominated by the clinkers and the SCMs mostly exert an indirect filler effect.

3.2.3 Early-stage glass dissolution and surface structure

The early-stage dissolution of two CAS glasses with compositions of a blast-furnace slag and a Si-rich fly ash at neutral and high alkaline conditions (pH = 11 and 13) has been studied at far from equilibrium conditions (solution/solid ratio of 10.000) by Newlands *et al*. [99,100]. Both glasses showed a preferential release of Ca over Si and Al at the very early stage of dissolution at neutral pH values whereas at high pH the elemental release rates were congruent. Estimation of the equivalent dissolved layer thicknesses, from the measured concentration of elements after 5 min of dissolution,

reveals the largest dissolved layer for Ca, which is less dependent of pH (*i.e.* 70 – 200 nm). In contrast, the dissolved layer thickness increases significantly for Si (and Al) from neutral to pH = 13 conditions for both glasses, *e.g.*, an increase in equivalent dissolved Si-layer thickness from roughly 5 up to 200 nm on going from pH = 6.2 to 13.0 for the slag-like glass [99]. The outer layers of the glasses exposed to dissolution for fixed times (5 – 180 min) were further analyzed after drying with the surface techniques ToF-SIMS and XPS which have different analytical depth resolutions of about 1.5 nm and 6 – 12 nm, respectively. In comparison with the bulk glass compositions, these experiments allowed a distinction of different surface compositions, at different penetration depths. For example, XPS showed a layer enriched in Si and Al for the BFS glass briefly exposed to pH neutral water whereas ToF-SIMS revealed a Ca surface enrichment. The XPS data reflect that the surface of BFS particles consist of a leached layer where the weakest bonded ions (Ca) and easily hydrolyzed species (Al) have been released to the solution. Mobile Ca and Al species are then accumulated at the surface of the leached layer or redeposited as a new phase to account for the Ca-enriched layer observed by ToF-SIMS.

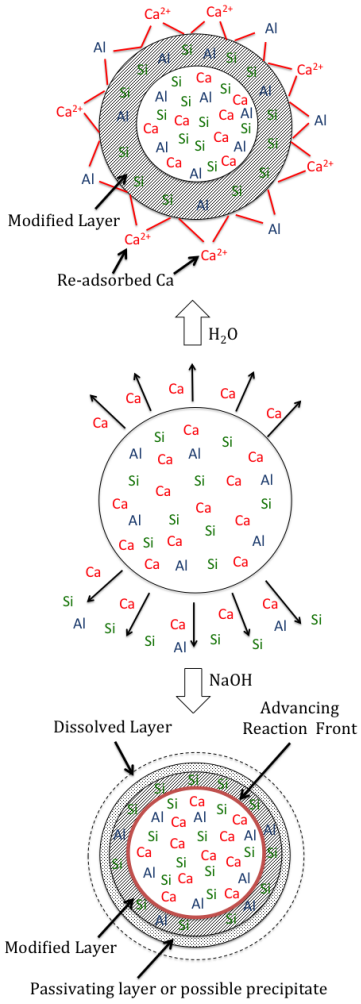

Fig. 5. Schematic representation of the glass surface structure for a CAS glass in diluted near-neutral and alkaline solutions. Reproduced with permission from ref. [99].

The results led to the proposed model for glass dissolution at neutral and highly alkaline conditions illustrated in Fig. 5. The glass dissolution is slow at near neutral pH conditions, resulting in a 'modified layer' rich in Si formed by the release of Ca^{2+} ions and hydrolyzed Al units. Hydrated Ca^{2+} ions and aluminate species will re-adsorb on the modified layer via cation-exchange reactions or electrostatic interactions between the negative surface and the positive ions. The glass dissolution is significantly enhanced at alkaline conditions with network hydrolysis and ion-exchange processes taking place at the same time, resulting in an increased release of silicate species to the solution. Deprotonation of the hydrated Ca^{2+} ions at high pH results in stronger interaction with the hydrolyzed silicate and aluminate species, which may lead to condensation reactions that may form a 'passivating layer' or 'precipitate' of low Ca/Si C-(A)-S-H at the front of the 'modified layer' (Fig. 5) [99]. A similar inhibiting effect of Ca concentration on glass dissolution rates was reported by Maraghechi *et al.* [40] for silica glass in 1 M NaOH and $Ca(OH)_2$ saturated solutions and by Chave *et al.* [104] for nuclear glass dissolution at near equilibrium conditions and high pH. Since the composition of the passivating surface layers in the quoted studies were dissimilar, it appears that the inhibiting effect is largely physical, caused by the adherent nanoporous nature of the surface alteration layer.

The effect of pH on the surface chemistry for synthesized calcium(-magnesium) aluminosilicate glasses with model compositions for blast furnace slags, fly ashes and silica fume has been investigated by 30 min batch pH titrations (pH ~ 2 – 12) and zeta potential measurements by Snellings [105]. These experiments showed that proton-metal exchange reactions are dominant at low pH (< 9), resulting in the formation of a leached layer rich in Si (in accord with Fig. 5). Moreover, the exchange reactions maintain the overall charge-balance, implying the absence of a re-polymerization of the silicate network in the leached layer. The proton-metal exchange rates decrease strongly at high pH where the overall proton mass balance is controlled by dissolution and hydrolysis of the released cations [105]. Thus, at high pH silica dissolution becomes more prominent than the proton-metal exchange reactions, resulting in a nearly congruent glass dissolution with the absence of a sizeable leached layer (Fig 6). Eventually, the increase in solution ionic concentrations may result in nucleation and growth of hydrate phases, leading in a positive feedback mechanism to a lowering in solution saturation and acceleration of dissolution. In glass dissolution studies such "resumption of dissolution" was observed to be triggered by precipitation of zeolites in Na-rich systems, smectites in Mg enriched systems and calcium silicate hydrates in Ca-rich systems. The reacceleration of dissolution occurs when the precipitates incorporate major glass forming network elements such as Al and Si [106]. In particular precipitation of Al strongly accelerates dissolution [107,108]. Fournier *et al.* [106] noted a loss of passivating properties of the glass alteration layer after consumption of the network forming elements by hydration productions.

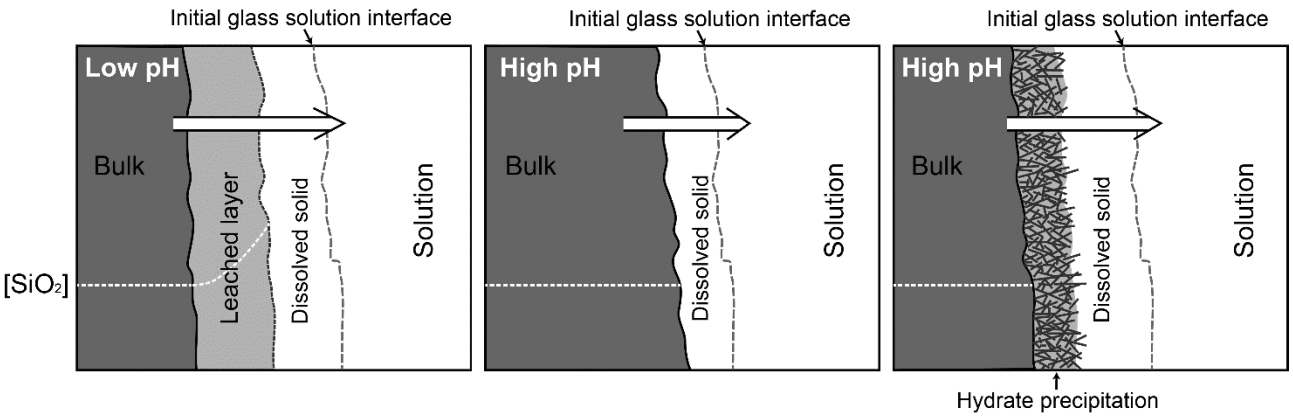

Fig. 6. Schematic representation of the evolution of the glass surface during initial dissolution at low vs. high pH on the left and the middle diagram, respectively. On the right-hand side, the eventual precipitation of hydrates leads to an acceleration of dissolution and a self-sustained hydration reaction. Reproduced with permission from ref. [105].

4. Impact of SCMs on blended cement hydration

4.1. Assessing SCM reactivity in blended cements

To accurately predict the hydration product assemblage of a blended cement over time, kinetic data on the hydration of all reactants, including the SCMs, is required. At present, such data need to be extracted from experiments or empirical models as reliably predicting reaction kinetics remains tedious for fundamental physics-based models, even for clinker phases, in complex blended cements [109,110]. The SCM reaction in Portland cement blends is generally promoted by alkalies and the presence of portlandite formed by the hydrating cement. Portlandite is crucial for the pozzolanic reaction of SCMs, and nearly all test methods for pozzolanic reactivity involve the chemical reaction of the SCM with $Ca(OH)_2$ [111,112]. The degree of SCM reaction under simple test conditions may differ significantly from physical performance results obtained for the SCM in real Portland cement blends. Probably for this reason, conventional compressive strength tests on Portland cement – SCM mortars are still widely used in the evaluation of SCM materials [113]. However, the SCM – portlandite based tests, where the degree of reaction is indirectly measured by the consumption of $Ca(OH)_2$, are generally less time-consuming, providing valuable measures for initial screening of materials and degrees of reaction independent of cement type. As a recent example of a new, alternative rapid screening procedure, the so-called R^3 test [114] simulates the reaction environment in a hydrating blended cement by curing the SCM at 40 ^{o}C in a solution with small amount of alkalis and sulfate ions in addition to $Ca(OH)_2$. The reaction progress is followed either by isothermal calorimetry or by determination of bound water up to 3 to 7 days of curing. Both measures have shown correlation with conventional 28 days compressive strengths for standard mortar bars for a

range of metakaolin-based SCMs [114] and also for a wider range of conventional SCMs, including slags, fly ashes, natural pozzolans and calcined clays [113].

A direct quantification of SCM reaction in Portland cement – SCM blends is often complicated by the reactive phases being amorphous in most SCMs, limiting the use of X-ray diffraction. Despite of that, progress in PONCKS analysis has also been reported for quantification of SCMs such as fly ashes, slags and calcined clays [115-117]. Alternatively, amorphous SCMs in cement blends may be studied by SEM backscattered electron (BSE) image analysis with EDS element mapping [118-120] or solid-state NMR spectroscopy [19,121,122]. For example, the elemental compositions of fly ashes, measured by SEM-EDS analysis of around 20.000 particles, were plotted into Ca-Al-Si ternary frequency plots by Durdzinski *et al*. [119], which allowed identification of four main groups of silicate phases with different Ca and Al contents. This classification was subsequently used to follow the hydration of fly ash in Portland cement blends, providing information about the reactivities of the main phases. ^{29}Si MAS NMR allows in several cases a clear distinction between the Portland clinkers and the SCM in blended cements, as utilized in studies of the degree of SCM reaction for Portland cement blends incorporating calcium aluminosilicate glasses [121], metakaolin [19] and calcined montmorillonite clay [122].

4.2 Effect of SCMs on early cement hydration

The impact of SCMs on the early cement hydration has been addressed in a study of C-S-H nucleation and growth by Berodier and Scrivener [123]. Using quartz powders with different fineness as an inert component in OPC blends with different replacement levels, they showed that the hydrate phases form in a similar way on both the surfaces of quartz and the cement grains (Fig. 7). In addition, it was found that the filler/cement ratio has only a small effect on the kinetics of early cement hydration. Similar results were observed for slag and fly ash, reflecting that these SCM particles are basically inert during the first day of hydration. The crucial parameter was found to be the interparticle distance, which depends on the fineness of the particles and the water/binder ratio. This was evidenced by a clear relationship between the slope of the calorimetry curves (main peak of the acceleration period) and the average distance between the particles. This relation was observed for plain cement and blended systems with different replacement levels and water/binder ratios, and found to be independent of the nature of the particles [123]. At the nano- to micrometer scale, diffusion of chemical species in the pore solution is very fast, making it unlikely this to be the rate-limiting factor. Instead, Berodier and Scrivener proposed that the accelerating effect of SCM addition is largely a mechanical effect of shearing between particles during mixing, which increases when the interparticle distance decreases, rather than an effect of additional surface available for C-S-H nucleation. Shearing may affect the double layer surrounding the cements grains and prevent accumulation of ions on the

interface of the surface. This effect has been observed in C_3S dissolution experiments at a high level of dilution using low stirring rates [124], while at the same time nuclei of C-S-H forming at the surface can be moved into solution, generating a seeding effect during the acceleration period. As an exception, limestone addition results in an accelerated hydration as compared to quartz. This was ascribed to increased nucleation of hydration products, potentially reflecting a favorable calcite surface structure for the C-S-H precipitation [123].

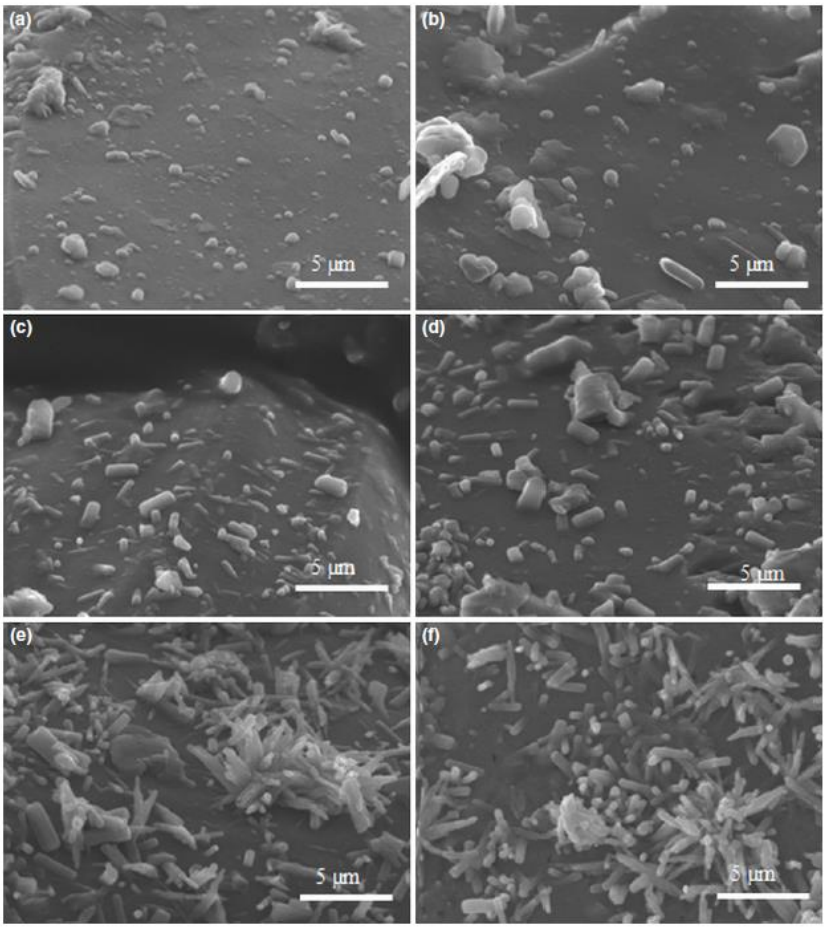

Fig. 7. SEM micrographs of an ordinary Portland cement – quartz paste, illustrating a similar growth of hydration products on the surfaces of quartz (a, d, e) and the cement gains (b, d, f) after hydration for 5 min (a, b), 2 hours (c, d) , and 5 hours (e, f). Reproduced with permission from ref. [123].

Accelerated cement hydration in blends with limestone rather than quartz has also been observed by Oey *et al.* [125]. They proposed that this effect is related to interfacial properties of the calcite surface, its ability to participate in ion-exchange reactions and a lower energy barrier for C-S-H nucleation compared to quartz from modelling of the heat profiles in calorimetric experiments. The affinity of the surfaces of ordinary Portland cement (OPC), micronized sand and limestone towards C-S-H

nucleation has been studied by zeta-potential measurements and SEM by Ouyang et al. [126], who also found that a much higher density of C-S-H nuclei was generated at the limestone surface after short hydration time. From the zeta-potential measurements, it was observed that the limestone surface has a much stronger affinity for Ca^{2+} ions than the silicate surfaces of micronized sand and OPC. The Ca^{2+} ions adsorb to the calcite surface by donor-acceptor mechanisms and their low mobility facilitates higher solution supersaturation and in consequence prolific formation of stable nuclei, followed by growth of C-S-H into macroscopic particles [126].

The influence of silica fume and metakaolin on the early-age hydration of triclinic C_3S has been investigated by calorimetric methods and simulations based on a phase boundary nucleation and growth model [127]. ~~Although~~ Silica fume accelerates C_3S hydration at low replacement levels, as a result of additional C-S-H nucleation sites. This effect may diminish at increasing silica fume contents as a result of a significant agglomeration of particles. ~~Coarser~~ The metakaolin particles were coarser than silica fume and found to be less susceptible to agglomeration. However, at increasing replacements aluminate ions released from metakaolin dissolution were postulated to inhibit dissolution of C_3S by inner-sphere surface complexation at reactive sites and poison growth of C-S-H nuclei [127]. Moreover, in addition to these effects and in line with the higher connectedness of their silicate structure, the dissolution rates for silica fume and metakaolin are lower than for C_3S, and thus silica fume and metakaolin were found only to have a minor impact on the early-age hydration kinetics for C_3S [127]. The inhibition of C_3S dissolution by aluminate ions in solution has been addressed in earlier studies of C_3S hydration kinetics and found to extend the induction period [128]. The inhibition is dependent of pH as well as the Ca^{2+} ion concentration in solution, and it is proposed that aqueous aluminate ions bind onto active dissolution sites at the C_3S surface. This view is supported by molecular dynamics simulations, which suggest that the aluminate ions interact with the hydroxylated C_3S surface and form ionic bonds with Ca^{2+} ions of the surface [129].

In addition to the intrinsic reactivity of the SCM and the filler effect, the reactivity in blended Portland cements depends also on the pore-solution chemistry. This has been addressed for the early hydration of binary OPC – SCM cements (50:50) by isothermal calorimetry and pore-solution analysis by Schöler *et al*. [130]. They found that changes in pore solution during the first 6 hours of hydration have the same effect on hydration kinetics as concentration changes observed for diluted systems. The principal parameter driving the hydration kinetics at early hydration is the degree of undersaturation of alite, which is affected by the type of added SCM. The C-S-H nucleation sites provided by limestone decrease the saturation of the pore solution with respect to C-S-H and results therefore in an accelerated hydration. On the other hand, early dissolution of fly ash increases the concentration of aluminate ions, which may hinder the dissolution of alite due to binding of aluminum on the alite surface sites, and thereby retards the hydration [128,130]. However, this process is also

dependent on the sulfate concentration in the pore solution as aluminate ions may efficiently be removed by ettringite precipitation. It has also been proposed that adsorption of Ca^{2+} ions on the fly ash slows down the silicate reaction [131] and thereby contributes to the retarding effect of fly ash on the early cement hydration. The effect of sulfate concentration and the alumina content of slag has been addressed for Portland cement – slags blends [132]. Here it was found that the alumina (and magnesia) from the slag has a major impact on the hydrate phase assemblage, in particular the AFm and AFt phases, whereas additional sulfate had an positive impact on the early-age strength.

4.3. Effect of SCMs on late cement hydration

The degree of reaction of the SCM and the level of SCM replacement in Portland cement – SCM blends have a significant impact on the phase assemblage and the composition of the C-(A)-S-H phase. This effect is most obvious after prolonged hydration. At later hydration ages, the increasing degree of SCM reaction results generally in increased amounts of dissolved aluminate and silicate species from the SCM. This affects the composition of the C-(A)-S-H phase. It decreases the Ca/Si ratio and increases the Al/Si ratio [19,133,134]. Moreover, a change in C-(A)-S-H morphology from fibrillar to foil-like morphology is observed for high replacement levels, as reported for slag and fly ash cement systems [135,136]. This may affect the effective density and space filling capacity of C-(A-)-S-H in blended cements.

The SCM reaction is strongly dependent on the dissolution and reaction of the cement, and competing reactions between the SCM and the clinker phases occur during hydration, reflecting differences in dissolution kinetics under the alkaline conditions. From dissolution data and other thermodynamic parameters, the hydrate phase assemblage in a hydrating system can be predicted by thermodynamic modelling approaches. Such tools, and the Gibbs free energy minimization software, GEMS [23,24] in particular, have been instrumental over the last decade in predicting the phase assemblages, porosity and volume stability and durability of blended cements in general (see ref. [137] for a very recent review). Thermodynamic modelling has also been employed in the assessment of SCM reactivity in blended cements, although the degree of reaction of the individual phases and the composition of the C-(A)-S-H phase require some restrictions in the modelling.

For a simple system such as Portland cement – silica fume, thermodynamic modelling predicts that increasing cement substitution gives increasing amounts of C-(A)-S-H as long as portlandite still is present [138]. After $Ca(OH)_2$ depletion the amount of C-(A)-S-H is nearly constant but the Ca/Si ratio of the C-(A)-S-H decreases, with increasing silica content, reflecting that dissolved silicate species react with already formed C-(A)-S-H. This in agreement with ^{1}H NMR relaxometry studies, where Ca/(Si + Al) ratios of 1.70 ± 0.02 [139] and 1.33 ± 0.02 [140] were reported for the C-(A)-S-H phase in pastes hydrated for 28 days of white Portland cement (wPc) and wPc – 10 wt.% silica

fume, respectively, while Al/Si = 0.05 was obtained from ^{29}Si NMR [140], *i.e.*, corresponding to Ca/Si ratios of 1.80 and 1.40. SEM-EDS and TEM studies of OPC hydration with increasing levels of silica fume have shown the existence of two different inner-product (IP) C-S-H rims where the outer rim, which is formed first and in the presence of portlandite, has a high Ca/Si ratio [141]. The second IP C-S-H rim has a lower Ca/Si ratio (down to ~ 1.0) and forms in the absence of portlandite at later ages, consuming calcium ions from the outer rim C-S-H. Pore solution studies for similar systems have reported a decrease in Ca concentration and pH and increase in Si concentration after portlandite has been depleted [142], which may influence the decrease in Ca/Si of the C-S-H under these conditions in blended cements.

For binary blends with an aluminosilicate-rich SCM such as metakaolin, thermodynamic modelling predicts the formation of strätlingite ($2CaO{\cdot}Al_2O_3{\cdot}SiO_2{\cdot}8H_2O$) when portlandite has depleted. Again, this is in full agreement with an experimental study of wPc blends with increasing metakaolin levels [19], where ^{27}Al NMR clearly revealed the presence of strätlingite above 15 wt% metakaolin for wPc – metakaolin pastes hydrated for up to 90 days. Moreover, the ^{29}Si NMR data for the same blends showed and almost linear increase in Al/Si ratio for the C-(A)-S-H phase with increasing metakaolin content and a decrease in Ca/Si ratio, as evidenced by longer aluminosilicate chain lengths [19]. The good agreement between the experimental and predicted phase assemblage for the wPc-metakaolin system probably reflects nearly full degrees of reaction for the principal phases (incl. metakaolin at substitution levels below 20 wt.%) after prolonged hydration (90 – 365 days) [19] and thereby a system close to 'global' thermodynamic equilibrium. However, in a hydration and mechanical performance study of ordinary Portland cement – metakaolin (0 – 40 wt.%) blends, the co-existence of the thermodynamically incompatible portlandite and strätlingite phases was found experimentally for blends with more than 20 wt.% metakaolin [14]. Their mutual presence was ascribed to the formation of a dense C-S-H matrix, resulting in a heterogeneous system where the phase assemblage is governed by local equilibria. The OPC contained a significant amount of belite (25 wt.%), which was found to react more slowly than metakaolin [14]. Thus, dissolution after longer hydration time will result in portlandite crystals that cannot necessarily be consumed by metakaolin reaction, as a result of space filling constraints. This may also contribute to heterogeneity in the system, which is not considered by conventional thermodynamic modelling.

The combination of thermodynamic modelling and experimental studies have been used to correlate microstructural parameters to mechanical properties such as compressive strength and elastic modulus for Portland cement – SCM blends, where a key-problem can be the determination of the degree of SCM reaction. For Portland cement - fly ash blends, Zajac and Ben Haha [143] have measured the dissolution of fly ash as a function of pH in NaOH solutions and used these data to estimate the degree of fly ash reaction in the blended cements, assuming that the fly ash dissolution

in the blends depends solely on the pH of the pore solution. The data was used to model the phase assemblage and volumetric evolution with hydration time, which gave good agreement with results from XRD on hydrate phases formed within 90 days of hydration. Moreover, the modelled volume changes (coarse porosities) correlated well with the measured compressive strength, suggesting that this is a valuable approach to engineer the performance of Portland cement – fly ash blends.

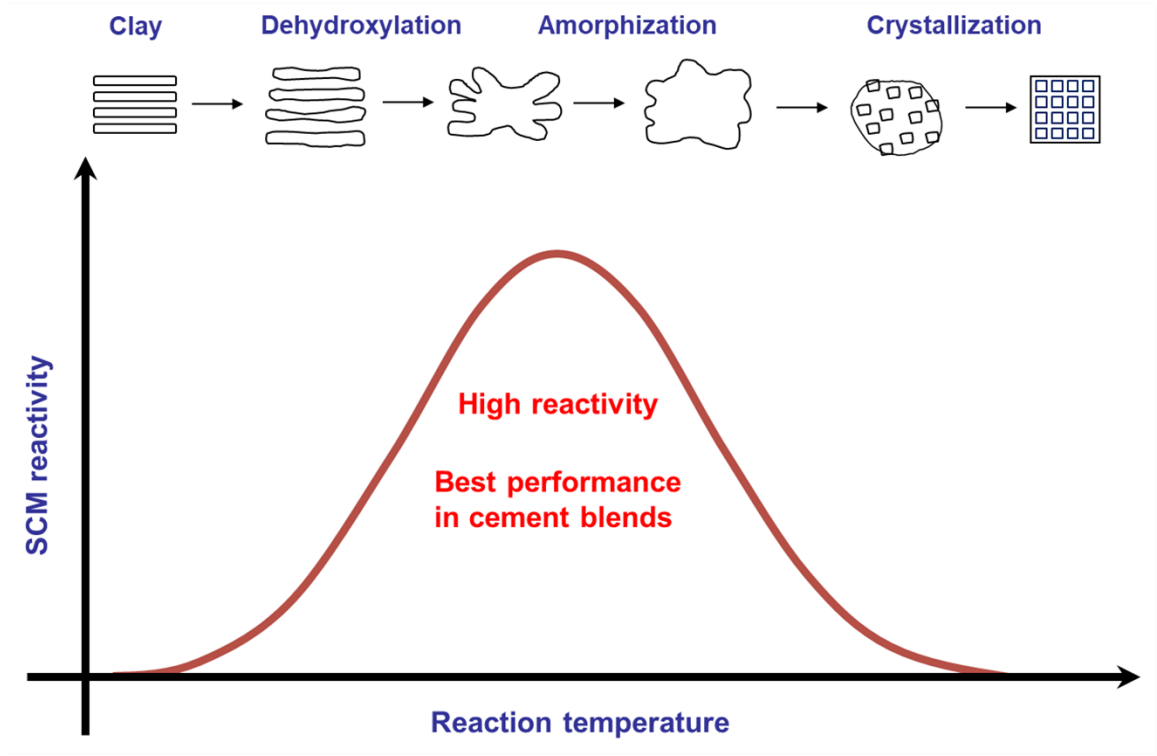

Fig. 8. Schematic diagram illustrating the different stages in heat-treatment of clay minerals.

5. Calcined clays as SCMs

Calcined clays are receiving increasing attention as possible replacements for slags and fly ashes, due to their wide abundance in the Earth's crust and rather low production costs relative to other alternative SCMs such as synthesized glasses. Calcined clays are amorphous aluminosilicate-rich materials with local structures that differ from the aluminosilicate network found in the active glassy phases of slags and fly ashes. Clay minerals or 'planar hydrous phyllosilicates' are generally composed of repeated tetrahedral (T) and octahedral (O) sheets which share a plane of oxygen atoms. The T sheet contains corner-sharing tetrahedral cations (*e.g.*, Si^{4+}, Al^{3+}, Fe^{3+}) whereas the O layer is formed by edge-sharing octahedral cations such as Al^{3+}, Fe^{3+}, Mg^{2+}, and Fe^{2+}. Clay minerals are classified as 1:1 (TO), 2:1 (TOT) or mixed-layer minerals, depending on their layer arrangement. The two most common minerals are kaolinite ($Si_2Al_2O_5(OH)_4$, 1:1 clay) and montmorillonite ($(M_y{\cdot}nH_2O)(Al_{2-y}Mg_y)Si_4O_{10}(OH)_2$; M = interlayer cations, 2:1 clay). Pozzolanic activity of clays can

generally be obtained by thermal activation, and highest reactivity is typically obtained for materials heat-treated at temperatures in the range 500 – 800 °C, well below temperatures of glass formation. The thermal transformation sequence for a natural clay is shown in Fig 8. Heat-treatment at low temperature results in dehydration by removal of water from the interlayers. This step is followed by a progressive dehydroxylation process where hydroxyl groups are removed and the layers collapse, forming an amorphous structure. The maximum pozzolanic reactivity is expected after heat-treatment at this stage, whereas higher temperatures will result in regain in structural order leading to crystallization of new distinct phases or glass formation.

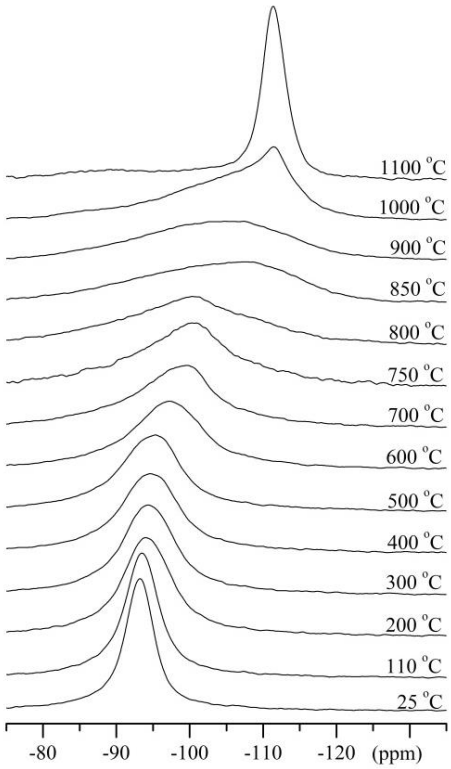

Fig. 9. ^{29}Si MAS NMR spectra (4.7 T) of a pure Ca-rich montmorillonite heated for 2 hours at temperatures in the range 25 – 1100 °C. Reproduced with permission from ref. [122].

Heat treatment of kaolinite results in a metastable phase, metakaolinite ('$Si_2Al_2O_7$'), which is stable over a rather large temperature range of approx. 450 – 850 °C with nearly the same amorphous/ disordered structure according to ^{27}Al and ^{29}Si NMR measurements [144,145]. A DFT study of the kaolinite – metakaolin transformation [146] has proposed that one out of eight hydroxyl H atoms remains in the metakaolin structure above the transformation temperature to prevent a complete collapse of the silica and alumina layers. On further heating (850 – 1100 °C), metakaolin transforms into mullite ($Al_2^{VI}(Al_{2+2x}^{IV}Si_{2-2x})O_{10-x}$) and amorphous silica, as seen by two distinct resonances at -97 and -110 ppm in the ^{29}Si MAS NMR spectra [145]. Metakaolin contains aluminum in four-, five-

and six-fold coordination and silicon in a range of different $Q^n(m\text{Al})$ SiO_4 environments. Metakaolin samples produced in the range 500 – 1100 ºC have been exposed to dissolution in HF solution and characterized by ^{27}Al and ^{29}Si MAS NMR [147]. These spectra and those of the solid residues from the dissolution experiments indicated the presence of at least seven different SiO_4 environments. Three sites of lower abundance corresponding to Q^4(0Al) and four sites to different types of $Q^3(m\text{Al})$ and $Q^4(m\text{Al})$ sites. Moreover, the spectra revealed that the Si sites with Al in the second coordination sphere are the most reactive sites in metakaolin.

The structural transformations upon heat-treatment for 2:1 clays such as montmorillonite [122] and illite/smectite [148] follow the scheme in Fig. 8. This includes steps of dehydration, dehydroxylation, amorphization and recrystallization, as illustrated by the ^{29}Si MAS NMR spectra of a heat-treated pure montmorillonite in Fig. 9. An important difference between the heat-treatment sequence for kaolinite and the 2:1 clay minerals is that a metastable phase is not observed for the 2:1 clay minerals. For montmorillonite, the ^{29}Si NMR spectra show a continuous change in resonance position and width up on heat treatment in the range 500 – 1000 ºC and that crystalline phase(s) start to form at 1000 ºC and above. The ^{29}Si resonance linewidths indicate the highest degree of disorder for samples heated at 800 – 1000 ºC, in good agreement with that ^{29}Si{^{1}H} CP/MAS NMR spectra of the samples show a full degree of dehydroxylation at 800 ºC [122]. Reactivity experiments ($Ca(OH)_2$ – calcined clay blends cured for 7 days at 40 ºC) for the samples show highest reactivity for calcination temperatures in a rather narrow range of ~750 – 850 ºC. Interestingly, the degree of clay reaction was observed to correlate with the Al/Si ratio of the produced C-(A)-S-H phase, indicating that high reactivity is associated with an increased release of aluminate ions into solution from the calcined clay [122].

The pozzolanic reactivities of a range of different clay minerals either in pure forms or in mixed materials from natural clay deposits have been addressed in a number of recent studies. These investigations have either used calcined clay – lime based test methods or studies of Portland cement – calcined clay blends [122,148-162], see also the compilations in refs. [163,164]. The studies reveal that the reactivity of calcined clays depends strongly on the clay mineralogy, the heat-treatment conditions, the purity of the clay sources and the Portland cement replacement level. The majority of studies have focused on metakaolin [150,153-155,158], which by far exhibits the highest pozzolanic reactivity of all clay minerals and is less sensitive to the temperature range of calcination. Most likely, this fact is related to increased dissolution rates of aluminate and silicate species from metakaolin, as compared to calcined 2:1 clays [165], which may reflect reminiscences of the original layer structures in the calcined materials. The octahedral layer of AlO_6 octahedra is sandwiched by layers of SiO_4 tetrahedra in 2:1 clays, which may screen the aluminate sites after heat treatment and inhibit their ability to undergo hydrolysis. On the other hand, the aluminate sites in metakaolin may be more

accessible as a result of the original 1:1 structure of SiO_4 tetrahedra and AlO_6 octahedra. In addition, the higher amount of hydroxyl groups in kaolinite, mainly present in the interlayers, may result in an increased loss of crystallinity upon dehydroxylation, which may favour pozzolanic reactivity, as proposed by Fernandez *et al*. [149].

The thermal activation and reactivity of kaolinite has been compared with smectitic (*e.g.*, montmorillonite) and illitic clays [149,156,161] either in blended cements or in calcined clay – lime blends. These studies reveal a high reactivity for kaolinite over a broad range of calcination temperatures (500 – 900 ^{o}C). The reactivity only exhibits a small dependence on the degree of local ordering, whereas much narrower ranges of optimum temperature around 800 – 900 ^{o}C are found for the smectitic and illitic clays. Moreover, the reactivity is found to decrease as follows: kaolinitic clays > Ca-montmorillonite > Na-montmorillonite > illite > hectorite [149,156]. This trend is largely also found for natural clays from industrial deposits, including mixed clay materials, when their potentials are evaluated by compressive strengths for OPC mortar samples with 20 and 40 wt.% replacements [160]. The presence of both kaolinite and bentonite (montmorillonite) in nearly equal amounts in natural clays have been addressed by Taylor-Lange *et al*. [152] and Alujas *et al*. [153]. Both studies reported that an interplay between dehydroxylation and recrystallization determines the calcination temperature for optimum reactivity. The specific surface area of the calcined clays decreases at high temperature and considering this effect on the pozzolanic activity as well, a temperature of 800 ^{o}C was found to represent the best compromise. Moreover, it was proposed that the pozzolanic reactivity is primarily driven by the metakaolin content, an effect which has been further investigated by Avet *et al*. [15,42] for Portland cement – calcined clay – limestone blends (LC^3) incorporating 30 and 50 wt.% calcined clay and limestone (2:1 ratio). The metakaolin content in different sources of calcined clay varied from 17 to 95%, and nearly a linear increase in compressive strength with calcined kaolinite content was observed for both cement blends at the studied hydration ages. This strongly suggests that secondary phases, such as other clay minerals or inert phases in clays, and factors such as fineness and calcination method only have a minor impact on the strength of the blends. For metakaolin contents above 40%, the compressive strengths were similar to those observed for pure Portland cement for both the blends with 30 and 50% replacement levels, demonstrating the potential of low-grade kaolinitic clays as SCMs. These findings were further supported by a range of microstructural analyses, which also showed that a metakaolin content above 65% in the calcined clay material retards the hydration of the clinker phases after approx. 3 days of hydration. Moreover, it results in a limited formation of calcium carboaluminate phases, most likely caused by the absence of capillary pores with a critical diameter above 3 – 5 nm [42].

One of the most important achievements in applications of calcined clays as SCMs is the development of ternary blends of Portland cement, limestone, and calcined clays. For these blends a

synergetic effect on compressive strength and durability is achieved for approx. 2:1 w/w combinations of calcined clay and limestone and cement replacement levels in the range 30 – 50 wt.% [166-168]. This synergetic effect has previously been observed for ternary blends of Portland cement and limestone with fly ashes [16,31,169], slags [10,169,170], and calcium aluminosilicate glasses [171,172] and may be expected for aluminosilicate-rich SCMs in general. In addition to the contribution of limestone as a filler, $CaCO_3$ reacts with alumina species in the pore solution and forms calcium hemi- and monocarboaluminate phases, which are high-volume, space-filling phases that reduce the porosity. This reaction stabilizes ettringite formed by alumina and the available sulfate ions, reducing porosity further and increasing the compressive strength [173]. The major part of studies of Portland cement – limestone – calcined clay blends have focused on rather pure metakaolin or calcined low-grade kaolinitic clays [15,42,166,168,174]. However, the synergetic effect has also been shown for ternary blends with calcined smectitic 2:1 type clays [169,175]. Variation of the ratio between limestone and calcined clay have shown optimum strength for w/w ratios of MK/(MK + LS) = 0.6 – 0.75 [166-168]. Thermodynamic modeling incorporating hydration kinetics, XRD as well as ^{27}Al and ^{29}Si NMR studies of ternary blends (35 wt% cement replacement level) with increasing MK/(MK + LS) ratios suggest that the optimum ratio corresponds to blends where nearly all $Ca(OH)_2$ has been consumed and strätlingite has not started to form yet [30].

Portland cement – limestone – calcined clay blends are frequently denoted LC^3 cements, which most often refer to the application of calcined low-grade kaolinitic clays. A review on such LC^3 cements considering the most crucial parameters for a sustainable blended cement, its production and technological properties as well as durability of the resulting concrete has recently presented [32].

5. Conclusions

Significant improvements in our understanding of SCM reactions, structure and compositions have been achieved over the last few years, in particular for SCMs such as fly ashes and slags, where the principal active components are glass-like phases. The use of calcium aluminosilicate glasses as model compounds has been beneficial in unravelling the mechanisms and parameters controlling SCM reactions in cement blends, employing concepts from geochemistry and thermodynamics as theoretical framework. Dissolution experiments of glasses have provided new insight into dissolution kinetics for the main elements and on the structure and compositions of glass particles in neutral and alkaline environments. Moreover, SCM dissolution makes a vital contribution to the pore-solution composition and its changes with hydration time. In blended cements at early hydration ages, the driving forces are primarily pH, water activity and pore-solution composition. Elements such as calcium and aluminum may have an inhibiting effect on the dissolution of active species from the surfaces of the clinkers and SCMs. At later hydration times, recent research has shown that the

presence of $Ca(OH)_2$ and water as well as space availability have decisive influence on hydration kinetics and the degree of reaction for the principal phases. In particular, pore refinement and the absence of capillary pores above a critical radius influence the hydration degrees and thereby affect the level of SCM substitutions in binary and ternary Portland cement blends.

Significant improvements in thermodynamic modelling of SCM in blended systems have been achieved over the last few years. However, more experimental data on structure, dissolution and kinetics are needed to obtain improved models that can account better for kinetics and allow prediction of fundamental materials properties of SCM blended systems. Such models can potentially be used in optimization of blended cements formulation in terms of physical performance, microstructure, durability and environmental footprint and thereby contribute to the most effective use of SCMs and cement clinkers. For kinetic studies of SCM reactivity, new or improved analytical techniques to describe and quantify amorphous phases and complex blends of phases with different structure or composition will be very helpful. In particular this holds for calcined clays, where fundamental knowledge on the structure and dissolution properties largely are lacking for the thermally activated phases. Finally, atomistic modelling tools have only been applied to a small extent in studies of SCM dissolution and hydrate growths on different surfaces, and it is foreseen that such approaches combined with advanced microscopic analytical tools can make important new contributions to our understanding of SCMs structure and reactivity.

References

[1] J.G.J. Olivier, G. Janssens-Maenhout, M. Muntean, J.A.H.W. Peters, Trends in global CO_2 emissions: 2015 report, The Hague: PBL Netherlands Environmental Assessment Agency; Ispra: European Commission, Joint Research Centre (2015).

[2] K.L. Scrivener, V. M. John, E.M. Gartner, "Eco efficient cements", United Nations Environment Program Sustainable Building and Climate Initiative (UNEP-SBCI), 2016.

[3] B. Lothenbach, G. Le Saout, E. Gallucci, K. Scrivener, Influence of limestone on the hydration of Portland cements, Cem. Concr. Res. 38 (2008) 848-860.

[4] R. Siddique, M. I. Khan, Supplementary Cementing Materials, Springer Science and Business Media, Berlin, 2011.

[5] B. Lothenbach, K. Scrivener, R.D. Hooton, Supplementary cementitious materials, Cem. Concr. Res. 41 (2011) 1244–1256.

[6] R. Snellings, G. Mertens, J. Elsen, Supplementary Cementitious Materials, Rev. Mineral. Geochemistry. 74 (2012) 211–278.

[7] K.-H. Yang, Y.-B. Jung, M.-S. Cho, S.-H. Tae, Effect of supplementary cementitious materials on reduction of CO_2 emissions from concrete. J. Clean. Prod. 103 (2015) 774-783.

[8] M.C.G. Juenger, R. Siddique, Recent advances in understanding the role of supplementary cementitious materials in concrete, Cem. Concr. Res. 78 (2015) 71-80.

[9] *First – Third International Conferences on Calcined Clays for Sustainable Concrete*, Lausanne, June 2015; Havanna, Cuba, December 2017; Delhi, India, October 2019. (see also refs. 163, 164).

[10] S. Adu-Amankwah, M. Zajac, C. Stabler, B. Lothenbach, L. Black, Influence of limestone on the hydration of ternary slag cements. Cem. Concr. Res. 100 (2017) 96-109.

[11] V. Kocaba, Development and evaluation of methods to follow microstructural development of cementitious systems including slags. PhD thesis No. 4523. EPFL, 2009.

[12] V. Kocaba, E. Gallucci, K. L. Scrivener. Methods for determination of degree of reaction of slag in blended cement pastes, Cem. Concr. Res. 42 (2012) 511-525.

[13] P.T. Durdziński, M. Ben Haha, S. A. Bernal, N. De Belie, E. Gruyaert, B. Lothenbach, E M. Méndez, J.L. Provis, A. Schöler, C. Stabler, Z. Tan, Y.V. Zaccardi, A. Vollpracht, F. Winnefeld, M. Zajac, K. L. Scrivener, Outcomes of the RILEM round robin on degree of reaction of slag and fly ash in blended cements, Mater. Struct. 50 (2017) 135.

[14] J. Skocek, M. Zajac, C. Stabler, M. Ben Haha, Predictive modelling of hydration and mechanical performance of low Ca composite cements: Possibilities and limitations from industrial perspective. Cem. Concr. Res. 100 (2017) 68 – 83.

[15] F. Avet, X. Li, K. Scrivener, Determination of the amount of reacted metakaolin in calcined clay blends. Cem. Concr. Res. 106 (2018) 40 – 48.

[16] K. De Weerdt, M. Ben Haha, G. Le Saout, K.O. Kjellsen, H. Justnes, B. Lothenbach, Hydration mechanisms of ternary Portland cements containing limestone powder and fly ash, Cem. Concr. Res. 41 (2011) 279–291.

[17] F. Deschner, B. Münch, F. Winnefeld, B. Lothenbach. Quantification of fly ash in hydrated, blended Portland cement pastes by backscattered electron imaging. J. Microscopy 251 (2013) 188-204.

[18] E. Berodier, K. Scrivener, Evolution of pore structure in blended systems. Cem. Concr. Res. 73 (2015) 25-35.

[19] Z. Dai, T.T. Tran, J. Skibsted, Aluminum incorporation in the C–S–H phase of white Portland cement–metakaolin blends studied by ^{27}Al and ^{29}Si MAS NMR spectroscopy, J. Am. Ceram. Soc. 97 (2014) 2662–2671.

[20] M.C.G. Juenger, R. Snellings, S.A. Bernal, Supplementary Cementitious materials: New Sources, characterization, and performance insights, Cem. Concr. Res. in press (2019).

[21] W.A. Gutteridge, J.A. Dalziel, Filler cement: The effect of the secondary component on the hydration of Portland cement. Part I. A fine non-hydraulic filler. Cem. Concr. Res. 20 (1990) 778 – 782.

[22] M. Cyr, P. Lawrence, E. Ringtot, Mineral admixtures in mortars: Quantification of the physical effect of inert materials on short-term hydration. Cem. Concr. Res. 35 (2005) 719-730.

[23] T. Wagner, D.A. Kulik, F.F. Hingerl, S.V. Dmytrieva, GEM-Selektor geochemical modeling package: TSolMod library and data interface for multicomponent phase models, Can. Mineral. 50 (2012) 1173-1195.

[24] D. Kulik, T. Wagner, S. Dmytrieva, G. Kosakowski, F. Hingerl, K. Chudnenko, U. Berner, GEM-Selektor geochemical modeling package: revised algorithm and GEMS3K numerical kernel for coupled simulation codes, Comput. Geosci. 17 (2013) 1-24.

[25] B. Lothenbach, D.A. Kulik, T. Matschei, M. Balonis, L. Baquerizo, B. Dilnesa, G.D. Miron, R.J. Myers,Cemdata18: A chemical thermodynamic database for hydrated Portland cements and alkali-activated materials. Cem. Concr. Res. 115 (2019) 472 – 506.

[26] J.W. Bullard, H. M. Jennings, R. A. Livingston, A. Nonat, G. W. Scherer, J. S. Schweitzer, K.L. Scrivener, J. Thomas, Mechanisms of cement hydration. Cem. Concr. Res. 41 (2011) 1208-1223.

[27] B. Lothenbach, Thermodynamic equilibrium calculations in cementitious systems. Mater. Struct. 43 (2010) 1413-1433.

[28] A. Vollpracht, B. Lothenbach, R. Snellings, J. Haufe, The pore solution of blended cements: a review. Mater. Struct. 49 (2016) 3341-3367.

[29] Scrivener, K.L., P. Juilland, P.J. Monteiro, Advances in understanding hydration of Portland cement. Cem. Concr. Res. 78 (2015) 38-56.

[30] W. Kunther, Z. Dai, and J. Skibsted, Thermodynamic modeling of hydrated white Portland cement–metakaolin–limestone blends utilizing hydration kinetics from ^{29}Si MAS NMR spectroscopy. Cem. Concr. Res. 86 (2016) 29-41.

[31] K. De Weerdt, K.O. Kjellsen, E. Sellevold, H. Justnes, Synergy between fly ash and limestone powder in ternary cements, Cem. Concr. Comp. 33 (2011) 30–38.

[32] K. Scrivener, F. Martinrena, S. Bishnoi, S. Maity, Calcined clay limestone cements (LC^3). Cem. Concr. Res. 114 (2018) 49-56.

[33] M. U. Okoronkwo, F.P. Glasser, Stability of strätlingite in the CASH system. Mater. Struct. 49 (2016) 4305-4318.

[34] A. Machner, M. Zajac, M. Ben Haha, K. O. Kjellsen, M. R. Geiker, K. De Weerdt, Limitations of the hydrotalcite formation in Portland composite cement pastes containing dolomite and metakaolin. Cem. Concr. Res. 105 (2018) 1-17.

[35] M. Zajac, P. Durdzinski, C. Stabler, J. Skocek, D. Nied, M. Ben Haha, Influence of calcium and magnesium carbonates on hydration kinetics, hydrate assemblage and microstructural development of metakaolin containing composite cements. Cem. Concr. Res. 106 (2018) 91-102.

[36] P. Lura, O.M. Jensen, K. van Breugel, Autogenous shrinkage in high-performance cement paste: An evaluation of basic mechanisms. Cem. Concr. Res. 33 (2003) 223-232.

[37] X. Wang, A.B. Eberhardt, E. Gallucci, K. Scrivener, Assessment of early age properties of cementitious system through isopropanol–water replacement in the mixing water. Cem. Concr. Res. 84 (2016) 76-84.

[38] T. Oey, A. Kumar, G. Falzone, J. Huang, S. Kennison, M. Bauchy, N. Neithalath, J. W. Bullard, G. Sant, The influence of water activity on the hydration rate of tricalcium silicate. J. Am. Ceram. Soc. 99 (2016) 2481-2492.

[39] R.J. Flatt, G.W. Scherer, J.W. Bullard, Why alite stops hydrating below 80% relative humidity. Cem. Concr. Res. 41 (2011) 987-992.

[40] H. Maraghechi, F. Rajabipour, C.G. Pantano, W. D. Burgos, Effect of calcium on dissolution and precipitation reactions of amorphous silica at high alkalinity. Cem. Concr. Res. 87 (2016) 1-13.

[41] G. W. Scherer, Crystallization in pores. Cem. Concr. Res. 29 (1999) 1347-1358.

[42] F. Avet, K. Scrivener, Investigation of the calcined kaolinite content on the hydration of Limestone Calcined Clay Cement (LC^3). Cem. Concr. Res. 107 (2018) 124-135.

[43] J. Bizzozero, C. Gosselin, K. L. Scrivener. Expansion mechanisms in calcium aluminate and sulfoaluminate systems with calcium sulfate. Cem. Concr. Res. 56 (2014)190-202.

[44] W. Huang, H. Kazemi-Kamyab, W. Sun, K. Scrivener, Effect of replacement of silica fume with calcined clay on the hydration and microstructural development of eco-UHPFRC. Mater. Design, 121 (2017) 36-46.

[45] J. D. Rimstidt, Geochemical rate models: an introduction to geochemical kinetics. 2014: Cambridge University Press.

[46] R. Snellings, Assessing, understanding and unlocking supplementary cementitious materials. RILEM Technical Letters, 1 (2016) 50-55.

[47] S. Abd.El.Aleem, M. Heikal, W. M. Morsi, Hydration characteristic, thermal expansion and microstructure of cement containing nano-silica, Constr. Build. Mater. 59 (2014) 151-160.

[48] H. Asgari, A. Ramezanianpour, H.-J. Butt, Effect of water and nano-silica solution on the early stages cement hydration, Constr. Build. Mater. 129 (2016) 11-24.

[49] M. Rupasinghe, R. San Nicolas, P. Mendis, M. Sofi, T. Ngo, Investigation of strength and hydration characteristics in nano-silica incorporated cement paste, Cem. Concr. Comp. 80 (2017) 17 - 30.

[50] F. Lavergne, R. Belhadi, J. Carriat, A. Ben Fraj, Effect of nano-silica particles on the hydration, the rheology, and strength development of a blended cement paste. Cem. Concr. Comp. 95 (2019) 42-55.

[51] W. Li, X. Li, S.J. Chen, G. Long, Y. M. Liu, W. H. Duan, Effects of nanoalumina and graphene oxide on early-age hydration and mechanical properties of cement paste, J. Mater. Civ. Eng. 29 (2017) 04017087.

[52] J. Zhou, K. Zheng, Z. Liu, F. He, Chemical effect of nano-alumina on early-age hydration of Portland cement. Cem. Concr. Res. 116 (2019) 159-167.

[53] R. Walker, S. Pavía, Physical properties and reactivity of pozzolans, and their influence on the properties of lime-pozzolan pastes, Mater. Struct. 44 (2011) 1139-1150.

[54] G. Quercia, G. Hüsken, H.J.H. Brouwers, Water demand of amorphous nano silica and its impact on the workability of cement paste. Cem. Concr. Res. 42 (2012) 344 – 357.

[55] E.C. Tsardaka, M. Stefanidou, Application of an alternative way for silica fume dispersion in cement pastes without ultrasonication. Cem. Concr. Res. 115 (2019) 59 – 69.

[56] M. Mirzahosseini, K. A. Riding, Influence of different particle sizes on reactivity of finely ground glass as supplementary cementitious material (SCM), Cem. Concr. Comp. 56 (2015) 95 – 105.

[57] S. Seraj, R. Cano, R. D. Ferron, M.C.G. Juenger, The role of particle size on the performance of pumice as a supplementary cementitious material. Cem. Concr. Comp. 80 (2017) 135 – 142.

[58] S. Liu, T. Zhang, Y. Guo, J. Wei, Q. Yu, Effects of SCMs particles on the compressive strength of micro-structurally designed cement paste: inherent characteristic effect, particle sizes refinement effect and hydration effect, Powder Techn. 330 (2018) 1 - 11.

[59] E. Lang, Blastfurnace cements. In: J. Bensted, P. Barnes (eds). Structure and Performance of Cements, London: Spon Press; 2002, 310 – 315.

[60] M. Moesgaard, D. Herfort, J. Skibsted, Y. Yue, Calcium alumino-silicate glasses as supplementary cementitious materials, Glass Technol. Eur. J. Glass Sci. Techn. Part A 51 (2010) 183 – 190.

[61] F. Winnefeld, M. Ben Haha, G. Le Saout, M. Costoya, S.-C. Ko, B. Lothenbach, Influence of slag composition on the hydration of alkali-activated slags, J. Sustain. Cement-Based Mater. 4 (2015) 85 – 100.

[62] T. Oey, A. Kumar, I. Pignatelli, Y. Yu, N. Neithalath, J. W. Bullard, M. Bauchy, G. Sant, Topological controls on the dissolution kinetics of glassy aluminosilicates. J. Am. Ceram. Soc. 100 (2017) 5521-5527.

[63] P.T. Durdzinski, C.F. Dunant, M. Ben Haha, K. L. Scrivener, A new quantification method based on SEM-EDS to assess the fly ash composition and study the reaction of its individual components in hydrating cement paste, Cem. Concr. Res. 73 (2015) 111 – 122.

[64] P.T. Durdzinski, R. Snellings, C.F. Dunant, M. Ben Haha, K.L. Scrivener, Fly ash as an assemblage of model Ca-Mg-Na-aluminosilicate glasses, Cem. Concr. Res. 78 (2015) 263-272.

[65] K.L. Aughenbaugh, P. Stutzman, M.c.G. Juenger, Identifying glass compositions in fly ash. Front. Mater. 3 (2016) 1.

[66] S. Kucharczyk, M. Zajac, C. Stabler, R. M. Thomsen, M. Ben Haha, J. Skibsted, J. Deja, Structure and reactivity of synthetic CaO-Al_2O_3-SiO_2 glasses, Cem. Concr. Res. 120 (2019) 77 - 91.

[67] A. Peys, C.E. White, D. Olds, H. Rahier, B. Blanpain, Y. Pontikes, Molecular structure of $CaO–FeO_x–SiO_2$ glassy slags and resultant inorganic polymer binders. J. Am. Ceram. Soc. 101 (2018) 5846-5857.

[68] L. Kriskova, M. Eroli, R.I. Iacobescu, S. Onisei, F. Vecchiocattivi, Y. Pontikes, Transformation of stainless steel slag toward a reactive cementitious binder. J. Am. Ceram. Soc. 101 (2018) 1727-1736.

[69] L. Kriskova, Y. Pontikes, L. Pandelaers, Ö. Cizer, P. T. Jones, K. Van Balen, B. Blanpain, Effect of high cooling rates on the mineralogy and hydraulic properties of stainless steel slags. Metallur. Mater. Trans. B, 44 (2013) 1173-1184.

[70] Y. Pontikes, L. Machiels, S. Onisei, L. Pandelaers, P.T. Jones, B. Blanpain, Slags with a high Al and Fe content as precursors for inorganic polymers. Appl. Clay Sci. 73 (2013) 93-102.

[71] P. Kinnunen, H. Sreenivasan, C.R. Cheeseman, M. Illikainen, Phase separation in alumina-rich glasses to increase glass reactivity for low-CO2 alkali-activated cements. J. Clean. Prod. 213 (2019) 126-133.

[72] P. Frugier, S. Gin, Y. Minet, T. Chave, B. Bonin, N. Godon, J.-E. Lartigue, P. Jollivet, A. Ayral, L. De Windt, G. Santarini, SON68 nuclear glass dissolution kinetics: Current state of knowledge and basis of the new GRAAL model. J. Nucl. Mater. 380 (2008) 8-21.

[73] S.L. Brantley, J.D. Kubicki, A.F. White, Kinetics of water-rock interaction. Springer NY, 2008.

[74] J. Schott, O.S. Pokrovsky, E.H. Oelkers, The link between mineral dissolution/precipitation kinetics and solution chemistry. Rev. Miner. Geochem. 70 (2009) 207-258.

[75] P. Aagaard, H.C. Helgeson, Thermodynamic and kinetic constraints on reaction rates among minerals and aqueous solutions; I, Theoretical considerations. Am. J. Sci. 282 (1982) 237-285.

[76] A. C. Lasaga, Transition state theory. Rev. Mineral. (United States), vol. 8, 1981.

[77] J.D. Rimstidt, H. Barnes, The kinetics of silica-water reactions. Geochim. Cosmochim. Acta, 44 (1980) 1683-1699.

[78] P.M. Dove, N. Han, A.F. Wallace, J. J. De Yoreo, Kinetics of amorphous silica dissolution and the paradox of the silica polymorphs. Proc. Nat. Acad. Sci. 105 (2008) 9903-9908.

[79] T. Burch, K. Nagy, A. Lasaga, Free energy dependence of albite dissolution kinetics at 80 C and pH 8.8. Chem. Geol. 105 (1993) 137-162.

[80] R. Hellmann, D. Tisserand, Dissolution kinetics as a function of the Gibbs free energy of reaction: An experimental study based on albite feldspar. Geochim. Cosmochim. Acta, 70 (2006) 364-383.

[81] A.C. Lasaga, A. Luttge, Variation of crystal dissolution rate based on a dissolution stepwave model. Science, 291 (2001) 2400-2404.

[82] A.C. Lasaga, A.E. Blum, Surface chemistry, etch pits and mineral-water reactions. Geochim. Cosmochim. Acta 50 (1986) 2363-2379.

[83] W. Stumm, G. Furrer, B. Kunz, The role of surface coordination in precipitation and dissolution of mineral phases. Croatica Chemica Acta, 56 (1983) 593-611.

[84] A. Blum, A. Lasaga, Role of surface speciation in the low-temperature dissolution of minerals. Nature, 331 (1988) 431.

[85] E.H. Oelkers, J. Schott, J.-L. Devidal, The effect of aluminum, pH, and chemical affinity on the rates of aluminosilicate dissolution reactions. Geochim. Cosmochim. Acta, 54 (1994) 2011-2024.

[86] E.H. Oelkers, General kinetic description of multioxide silicate mineral and glass dissolution. Geochim. Cosmochim. Acta, 65 (2001) 3703-3719.

[87] E.H. Oelkers, S.R. Gislason, The mechanism, rates and consequences of basaltic glass dissolution: I. An experimental study of the dissolution rates of basaltic glass as a function of aqueous Al, Si and oxalic acid concentration at 25 C and pH = 3 and 11. Geochim. Cosmochim. Acta, 65 (2001) 3671-3681.

[88] J.D. Kubicki, L.M. Schroeter, M.J. Itoh, B.N. Nguyen, S.E. Apitz, Attenuated total reflectance Fourier-transform infrared spectroscopy of carboxylic acids adsorbed onto mineral surfaces. Geochim. Cosmochim. Acta 63 (1999) 2709-2725.

[89] J.D. Kubicki, D. Sykes, S. Apitz, Ab Initio Calculation of Aqueous Aluminum and Aluminum - Carboxylate Complex Energetics and ^{27}Al NMR Chemical Shifts. J. Phys. Chem. A, 103 (1999) 903-915.

[90] J.P. Icenhower, P.M. Dove, The dissolution kinetics of amorphous silica into sodium chloride solutions: effects of temperature and ionic strength. Geochim. Cosmochim. Acta, 64 (2000) 4193-4203.

[91] J.-M. Gautier, E.H. Oelkers, J. Schott, Experimental study of K-feldspar dissolution rates as a function of chemical affinity at 150 C and pH 9. Geochim. Cosmochim. Acta, 58 (1994) 4549-4560.

[92] B.R. Bickmore, K.L. Nagy, A. K. Gray, A. R. Brinkerhoff, The effect of $Al(OH)_4^-$ on the dissolution rate of quartz. Geochim. Cosmochim. Acta, 70 (2006) 290-305.

[93] W. Stumm, G. Furrer, E. Weiland, B. Zinder, The effects of complex-forming ligands on the dissolution of oxides and aluminosilicates, in: The chemistry of weathering. Ed. J.I. Drever, 1985, Springer. p. 55-74.

[94] L.J. Criscenti, J.D. Kubicki, S.L. Brantley, Silicate glass and mineral dissolution: calculated reaction paths and activation energies for hydrolysis of a Q^3 Si by H_3O^+ using ab initio methods. J. Phys. Chem. A, 110 (2006) 198-206.

[95] A. Pelmenschikov, J. Leszczynski, L.G. Pettersson, Mechanism of dissolution of neutral silica surfaces: Including effect of self-healing. J. Phys. Chem. A, 105 (2001) 9528-9532.

[96] A.F. White, S.L. Brantley, Chemical weathering rates of silicate minerals. Vol. 31. 2018: Walter de Gruyter GmbH & Co KG.

[97] H.R. Westrich, R. T. Cygan, W. H. Casey, C. Zemitis, G.W. Arnold, The dissolution kinetics of mixed-cation orthosilicate minerals. Am. J. Sci. 293 (1993) 869-893.

[98] R. Snellings, Solution-controlled dissolution of supplementary cementitious material glasses at pH 13: the effect of solution composition on glass dissolution rates, J. Am. Ceram. Soc. 96 (2013) 2467 – 2475.

[99] K. C. Newlands, M. Foss, T. Matchei, J. Skibsted, D. E. Macphee, Early stage dissolution characteristics of alumino silicate glasses with blast furnace slag- and fly-ash-like compositions, J. Am. Ceram. Soc. 100 (2017) 1941 – 1955.

[100] K. C. Newlands, D. E. Macphee, The reactivity of aluminosilicate glasses in cements – effects of Ca content on dissolution characteristics and surface precipitation. Adv. Appl. Ceram. 116 (2017) 216 – 224.

[101] A. Schöler, F. Winnefeld, M. Ben Haha, B. Lothenbach, The effect of glass composition on the reactivity of synthetic glasses. J. Am. Ceram. Soc. 100 (2017) 2553 – 2567.

[102] Snellings, R., H. Kazemi-Kamyab, and K. Ferrand, Dissolution and reaction rates of waste materials in cement: temperature dependence, in 4th International Workshop on Mechanisms and Modelling of Waste / Cement Interactions. 2016, EMPA: Murten.

[103] J.L. Poole, K.A. Riding, K.J. Folliard, M.C.G. Juenger, A.K. Schindler, Methods for calculating activation energy for Portland cement. ACI Mater. J. 104 (2007) 303-311.

[104] T. Chave, P. Frugier, S. Gin, A. Ayral, Glass–water interphase reactivity with calcium rich solutions. Geochim. Cosmochim. Acta, 75 (2011) 4125-4139.

[105] R. Snellings, Surface chemistry of calcium aluminosilicate glasses. J. Am. Ceram. Soc. 98 (2015) 303 – 314.

[106] M. Fournier, S. Gin, P. Frugier, Resumption of nuclear glass alteration: state of the art. J. Nucl. Mater. 448 (2014) 348-363.

[107] P. Frugier, M. Fournier, S. Gin, Modeling resumption of glass alteration due to zeolites precipitation. Proc. Earth Planet. Sci. 17 (2017) 340-343.

[108] M. Fournier, S. Gin, P. Frugier, S. Mercado-Depierre, Contribution of zeolite-seeded experiments to the understanding of resumption of glass alteration. npj Materials Degradation, 1 (2017) 17.

[109] L. Valentini, Modeling dissolution–precipitation kinetics of alkali-activated metakaolin. ACS Omega, 3 (2018) 18100-18108.

[110] J. W. Bullard, E.J. Garboczi, P. E. Stutzman, P. Feng, A. S. Brand, L. Perry, J. Hagedorn, W. Griffin, J.E. Terril, Measurement and modeling needs for microstructure and reactivity of next-generation concrete binders. Cem. Concr. Compos. 101 (2019) 24–31.

[111] K.L. Scrivener, B. Lothenbach, N. de Belie, E. Gruyaert, J. Skibsted, R. Snellings, A. Vollpracht, TC 238-SCM: hydration and microstructure of concrete with SCMs: State of the art on methods to determined degree of reaction of SCMs, Mater. Struc. 48 (2015) 835 – 862.

[112] R. Snellings, K. L. Scrivener, Rapid screening tests for supplemnetary cementitious materials: past and future, Mater. Struc. 49 (2016) 3265 – 3279.

[113] X. Li, R. Snellings, M. Antoni, N.M. Alderete, M. Ben Haha, S. Bishnoi, Ö. Cizer, M. Cyr, K. De Weerdt, Y. Dhandapani, J. Duchesne, J. Haufe, D. Hooton, M. Juenger, S. Kamali Bernard, S. Kramar, M. Marroccoli, A.M. Joseph, A. Parashar, C. Patapy, J.L. Provis, S. Sabio, M. Santhanam, L. Steger, T. Sui, A. Telesca, A. Vollpracht, F. Vargas, B. Walkley, F. Winnefeld, G. Ye, M. Zajac, S. Zhang, K.L. Scrivener, Reactivity tests for supplementary cementitious materials: RILEM TC 267-TRM phase 1, Mater. Struct. 51 (2018) 151.

[114] F. Avet, R. Snellings, A. Alujas Diaz, M. Ben Haha, K. Scrivener, Development of a new rapid, relevant and reliable (R^3) test method to evaluate the pozzolanic reactivity of calcined kaolinitic clays, Cem. Concr. Res. 85 (2016) 1–11.

[115] R. Snellings, A. Salze, K.L. Scrivener, Use of X-ray diffraction to quantify amorphous supplementary cementitious materials in anhydrous and hydrated blended cements, Cem. Concr. Res. 64 (2014) 89 – 98.

[116] Y.P. Stetsko, N. Shanahan, H. Deford, A. Zayed, Quantification of supplementary cementitious content in blended Portland cement using an iterative Rietveld - PONKCS technique, J. Appl. Cryst. 50 (2017) 498 – 507.

[117] G. B. Singh, K. Subramaniam, method for direct determination of glassy phase dissolution in hydrating fly ash-cement system using x-ray diffraction, J. Am. Ceram. Soc. 100 (2017) 403-412.

[118] P.T. Durdzinski, C.F. Dunant, M. Ben Haha, K. L. Scrivener, A new quantification method based on SEM-EDS to assess the fly ash composition and study the reaction of its individual components in hydrating cement paste, Cem. Concr. Res. 73 (2015) 111 – 122.

[119] P.T. Durdzinski, M. Ben Haha, M. Zajac, K. L. Scrivener, Phase assemblage of composite cements, Cem. Concr. Res. 99 (2017) 172-182.

[120] J. Pfingsten, J. Rickert, K. Lipus, Estimation of the content of ground granulated blast furnace slag and different pozzolanas in hardened cement, Constr. Build. Mater. 165 (2018) 931 – 938.

[121] M. Moesgaard, S.L. Poulsen, D. Herfort, M. Steenberg, L.F. Kirkegaard,. J. Skibsted, Y. Yue, Hydration of Blended Portland Cements Containing Calcium-Aluminosilicate Glass Powder, J. Am. Ceram. Soc. 95 (2012) 403 – 409.

[122] N. Garg, J. Skibsted, Thermal activation of a pure montmorillonite clay and its reactivity in cementitious systems, J. Phys. Chem. C 118 (2014) 11464–11477.

[123] E. Berodier, K. Scrivener, Understanding the filler effect on nucleation and growth of C-S-H. J. Am. Ceram. Soc. 97, 3764 – 3773 (2014).

[124] L. Nicoleau, A. Nonat, D. Perrey, The di- and tricalcium silicate dissolutions, Cem. Concr. Res. 47 (2013) 14 – 30.

[125] T. Oey, A. Kumar, J. W. Bullard, N. Neithalath, G. Sant, The filler effect: the influence of filler content and surface area on cementitious reaction rates. J. Am. Ceram. Soc. 96 (2013) 1978 – 1990.

[126] X. Ouyang, D. A. Koleva, G. Ye, K. van Breugel, Insights into the mechanism of nucleation and growth of C-S-H on fillers. Mater. Struct. 50 (2017) 213.

[127] J. Lapeyre, A. Kumar, Influence of pozzolanic additives on hydration mechanisms of tricalcium silicate. J. Am. Ceram. Soc. 101 (2018) 3557 – 3574.

[128] L. Nicoleau, E. Schreiner, A. Nonat, Ion-specific effects influencing the dissolution of tricalcium silicate. Cem. Concr. Res. 59 (2014) 118- 138.

[129] E. Pustovgara, R.K. Mishra, M. Palacios, J.B. d'Espinose de Lacaillerie, T. Matchei, A.S. Andreev, H. Heinz, R. Verel, R.J. Flatt, Influence of aluminates on the hydration kinetics of tricalcium silicate. Cem. Concr. Res. 100 (2017) 245- 262.

[130] A. Schöler, B. Lothenbach, F. Winnefeld, M. Ben Haha, M. Zajac, H.-M. Ludwig, Early hydration of SCM-blended Portland cements: A pore solution and isothermal calorimetry study. Cem. Concr. Res. 93 (2017) 71 – 82.

[131] S. Dittrich, J. Neubauer, F. Goetz-Neunhoeffer, The influence of fly ash on the hydration of OPC within the first 44 h – A quantitative in situ XRD and heat flow calorimetry study. Cem. Concr. Res. 56 (2014) 129 – 138.

[132] M. Whittaker, M. Zajac, M. Ben Haha, F. Bullerjahn, L. Black, The role of the alumina content of slag, plus the presence of additional sulfate on the hydration and microstructure of Portland cement-slag blends. Cem. Concr. Res. 66 (2014) 91 -101.

[133] J. I. Escalante-Garcia, J. H. Sharp, The chemical composition and microstructure of hydration products in blended cements. Cem. Concr. Com. 26 (2004) 967-976.

[134] I. G. Richardson, "Tobermorite/Jennite and Tobermorite/Calcium Hydroxide-Based Models for the Structure of C-S-H: Applicability to Hardened Pastes of Tricalcium Silicate, b-Dicalcium Silicate, Portland Cement, and Blends of Portland Cement with Blast-Furnace Slag, Metakaolin, or Silica Fume", Cem. Concr. Res. 34 (2004) 1733–1777.

[135] R. Taylor, I.G. Richardson, R.M.D. Brydson, Composition and microstructure of 20-year-old ordinary Portland cement–ground granulated blast-furnace slag blends containing 0 to 100% slag. Cem. Concr. Res. 40 (2010) 971–983.

[136] I.G. Richardson, A.V. Girão, R. Taylor, S. Jia, Hydration of water- and alkali-activated white Portland cement pastes and blends with low-calcium pulverized fuel ash. Cem. Concr. Res. 83 (2016) 1 – 18.

[137] B. Lothenbach, M. Zajac, Application of thermodynamic modelling to hydrated cements. Cem. Concr. Res. (in press 2019).

[138] W. Kunther, S. Ferreiro, J. Skibsted, Influence of the Ca/Si ratio on the compressive strength of cementitious calcium-silicate-hydrate binders, J. Mater. Chem. A 5 (2017) 17401 – 17412.

[139] A.C.A. Muller, K.L. Scrivener, A.M. Gajewicz, P.J. McDonald, Densification of C-S-H measured by ^{1}H NMR relaxometry. J. Phys. Chem. C 117 (2013) 403–412.

[140] A.C.A. Muller, K.L. Scrivener, J. Skibsted, A.M. Gajewicz, P.J. McDonald, Influence of silicate fume on the microstructure of cement pastes: new insights from ^{1}H NMR relaxometry. Cem. Concr. Res. 74 (2015) 116 – 125.

[141] J.E. Rossen, B. Lothenbach, K.L. Scrivener, Composition of C-S-H in pastes with increasing levels of silica. Cem. Concr. Res. 75 (2015) 14-22.

[142] T.T.H. Bach, C.C.D. Coumes, I. Pochard, C. Mercier, B. Revel, A. Nonat, Influence of temperature on the hydration products of low pH cements, Cem. Concr. Res. 42 (2012) 805 – 817.

[143] M. Zajac, M. Ben Haha, Experimental investigation and modelling of hydration and performance evolution of fly ash cement. Mater. Struct. 47 (2014) 1259 – 1269.

[144] K.J.D. Mackenzie, I.W.M Brown, R.H. Meinhold, M.E. Bowden, Outstanding problems in the kaolinite-mullite sequence investigated by ^{29}Si and ^{27}Al solid state nuclear magnetic resonance: I, metakaolinite, J. Am. Ceram. Soc. 68 (1985) 293-297.

[145] D. Massiot, P. Dion, J.F. Alcover, F. Bergaya, ^{27}Al and ^{29}Si MAS NMR study of kaolinite thermal decomposition by controlled rate thermal analysis, J. Am. Ceram. Soc. 78 (1995) 2940 – 2944.

[146] C.E. White, J.L Provis, T. Proffen, D.P. Riley J.S.J Van Deventer, Density functional modelling of the local structure of kaolinite subjected to thermal dihydroxylation. J. Phys. Chem. A 114 (2010) 4988 – 4996.

[147] C. Ruiz-Santaquiteria, J. Skibsted, Identification of reactive sites in calcined kaolinite and montmorillonite from a combination of chemical methods and solid-state NMR spectroscopy. In Calcined Clays for Sustainable Concrete, RILEM Bookseries 16, Eds: F. Martirena, A. Favier, K. Scrivener (2018) pp. 404 – 408.

[148] N. Garg, J. Skibsted, Pozzolanic reactivity of a calcined interstratified illite/smectite (70/30) clay. Cem. Concr. Res. 79 (2016) 101 – 111.

[149] R. Fernandez, F. Martirena, K. L. Scrivener, The origin of the pozzolanic activity of calcined clay minerals: a comparison between kaolinite, illite and montmorillonite. Cem. Concr. Res. 41 (2011) 113 – 122.

[150] A. Tironi, M.A. Trezza, A.N. Scian, E.F. Irrasar, Kaolinitic calcined clays: factors affecting its performance as pozzolans. Constr. Build. Mater. 28 (2012) 276 – 281.

[151] A. Tironi, M.A. Trezza, A.N. Scian, E.F. Irrasar, Assessment of pozzolanic activity of different calcined clays. Cem. Concr. Comp. 37 (2013) 319-327.

[152] S. C. Taylor-Lange, E. L. Lamon, K.A. Riding, M.C.G. Juenger, Calcined kaolinite-bentonite clay blends as supplementary cementitious materials. Appl. Clay Sci. 108 (2015) 84 – 93.

[153] A. Alujas, R. Fernández, R. Quintana, K. L. Scrivener, F. Martirena, Pozzolanic reactivity of low grade kaolinitic clays: Influence of calcination temperature and impact of calcination products on OPC hydration. Appl. Clay Sci. 108 (2015) 94 – 101.

[154] A. Teklay, C. Yin, L. Rosendahl, L.L. Køhler, Experimental and modeling study of flash calcination of kaolinite rich clay particles in a gas suspension calciner. Appl. Clay Sci. 103 (2015) 10 – 19.

[155] A. Souri, H. Kazemi-Kamyab, R. Snellings, R. Naghizadeh, F. Golestani-Fard, K. Scrivener, Pozzolanic activity of mechanochemically and thermally activated kaolins in cement. Cem. Concr. Res. 77 (2015) 47 – 59.

[156] S. Hollanders, R. Adriaens, J. Skibsted, Ö. Cizer, J. Elsen, Pozzolanic reactivity of pure calcined clays. Appl. Clay Sci. 132 – 133 (2016) 552 – 600.

[157] J. Calabria-Holley, S. Papatzani, B. Naden, J. Mitchels, K. Paine, Taylored montmorillonite nanoparticles and their behaviour in the alkaline cement environment. Appl. Clay Sci. 143 (2017) 67-75.

[158] A. Tironi, F. Cravero, A.N. Scian, E.F. Irrasar, Pozzolanic activity of calcined halloysite-rich kaolinitic clays. Appl. Clay Sci. 147 (2017) 11-18.

[159] B. Bratoev, I. Doykov, J. Ninov, A. Lenchev, Pozzolanic activity assessment of calcined clays with complex minerals content. Adv. Cem. Res. 30 (2018) 103 – 122.

[160] S.E: Schulze, J. Rickert, Suitability of natural calcined clays as supplementary cementitious material. Cem. Concr. Comp. 95 (2019) 92-97.

[161] T. Danner, G. Norden, H. Justnes, Characterization of calcined raw clays as supplementary cementitious materials. App. Clay Sci. 162 (2018) 391 – 402.

[162] S. Ferreiro, M.M.C. Canut, J. Lund, D. Herfort, Influence of fineness of raw clay and calcination temperature on the performance of calcined clay-limestone blended cements. Appl. Clay Sci. 169 (2019) 81 – 90.

[163] K. Scrivener, A. Favier (Eds.), Calcined clays for sustainable concrete. Proceedings of the 1st International Conference on Calcined Clays for Sustainable Concrete. RILEM Bookseries 10, Springer 2015.

[164] F. Martirena, A. Favier, K. Scrivener (Eds.), Calcined clays for sustainable concrete. Proceedings of the 2st International Conference on Calcined Clays for Sustainable Concrete. RILEM Bookseries 16, Springer 2018.

[165] N. Garg and J. Skibsted, Dissolution kinetics of calcined kaolinite and montmorillonite in alkaline conditions: evidence for Al(V) sites, (under review 2019).

[166] M. Antoni, J. Rossen, K. Scrivener, R. Castillo, A. Alujas Diaz, F. Martirena, Investigation of cement substitution by combined addition of calcined clays and limestone, Proceedings of the XIII International Congress on the Chemistry of Cement, Madrid, July 3 – 8, 2011, p. 96 (7 pages).

[167] M. Steenberg, D. Herfort, S. L. Poulsen, J. Skibsted, J.S. Damtoft, Composite cement based on Portland cement clinker, limestone and calcined clay, Proceedings of the XIII International Congress on the Chemistry of Cement, Madrid, July 3 – 8, 2011, p. 97 (7 pages).

[168] M. Antoni, J. Rossen, F. Martirena, K. Scrivener, Cement substitution by a combination of metakaolin and limestone. Cem. Concr. Res. 42 (2012) 1579 – 1589.

[169] P. Mounanga, M. Khokhar, R. El. Hachem, A. Loukili, Improvement of the early-age reactivity of fly ash and blast furnace slag cementitious systems using limestone filler. Mater. Struct. 44 (2011) 437 – 453.

[170] A. Schöler, B. Lothenbach, F. Winnefeld, M. Zajac, Hydration of quarternary Portland cement blends containing blast-furnace slag, siliceous fly ash and limestone powder. Cem. Concr. Comp. 55 (2015) 374-382.

[171] M. Moesgaard, D. Herfort, M. Steenberg, L.F. Kirkegaard, Y. Yue, Physical performances of composite cements containing calcium aluminosilicate glass powder and limestone, Cem. Concr. Res. 41 (2011) 359 – 364.

[172] M. Moesgaard, S. L. Poulsen, D. Herfort, M. Steenberg, L. F. Kirkegaard, J. Skibsted, Y. Yue, Hydration of blended Portland cements containing calcium-aluminosilicate glass powder and limestone, J. Am. Ceram. Soc. 95 (2012) 403 – 409.

[173] T. Matchei, B. Lothenbach, F.P. Glasser, The role of calcium carbonate in cement hydration, Cem. Concr. Res. 37 (2007) 551-558.

[174] L.M.V. Andrés, M.G. Antoni, A.Alujas, J.F. Martirena, K. L. Scrivener, Effect of fineness in clinker-calcined clays-limestone cements. Adv. Cem. Res. 27 (2015) 546-556.

[175] S. Ferreiro, D. Herfort, J.S. Damtoft, Effect of raw clay type, fineness, water-to-cement ratio and fly ash addition on workability and strength performance of calcined clay – limestone Portland cements. Cem. Concr. Res. 101 (2017) 1 – 12.